이학박사 학위논문

Intravital imaging longitudinally monitors *in vivo* distributions and properties of the engrafted cells for stem cell therapy targeted to interstitial cystitis / bladder pain syndrome

간질성 방광염 / 방광 통증 증후군을 타겟으로 하는
줄기세포 치료를 위한 생체 내 분포 및
이식 된 세포의 특성 모니터링

울 산 대 학 교 대 학 원
의 학 과
류 채 민

간질성 방광염 / 방광 통증 증후군을 타겟으로 하는 줄기세포 치료를 위한 생체 내 분포 및 이식 된 세포의 특성 모니터링

지도교수 주 명 수

지도교수 신 동 명

이 논문을 이학박사 학위논문으로 제출함

2018 년 12 월

울 산 대 학 교 대 학 원

의 학 과

류 채 민

류채민의 이학박사학위 논문을 인준함

위 원 장 박 형 근 (인)

위 원 주 명 수 (인)

위 원 송 상 훈 (인)

위 원 신 동 명 (인)

위 원 오 승 준 (인)

울 산 대 학 교 대 학 원

2018 년 12 월

Doctor of Philosophy

Intravital imaging longitudinally monitors *in vivo* distributions and properties of the engrafted cells for stem cell therapy targeted to interstitial cystitis / bladder pain syndrome

The Graduate School

of the University of Ulsan

Department of Urology and Biomedical Sciences

Chae-Min, Ryu

Intravital imaging longitudinally monitors *in vivo* distributions and properties of the engrafted cells for stem cell therapy targeted to interstitial cystitis / bladder pain syndrome

Supervisor : Myung-Soo, Choo

Dong-Myung, Shin

Submitted to the Graduate School of University of Ulsan

In partial Fulfillment of the Requirements for the Degree of

Doctor of Philosophy in Medical Science at College of Medicine

by

Chae-Min, Ryu

Department of Biomedical Sciences

Ulsan, Korea

December 2018

ABSTRACT

Mesenchymal stem cells (MSC) have been considered as a novel therapeutic approach for interstitial cystitis/bladder pain syndrome (IC/BPS), which is an intractable disease characterized by severe pelvic pain and urinary frequency. However, little direct analysis of *in vivo* properties of the transplanted cells hampers the precise understanding of their underlying therapeutic mechanisms after transplantation and developing optimal transplantation protocols. Here, we showed the *in vivo* distribution and perivascular integration of human embryonic stem-cell (hESC) derived multipotent stem-cell (M-MSC) in living animals and their improved therapeutic outcomes in a lipopolysaccharide (LPS) instillation-induced IC/BPS animal model.

A novel combination of longitudinal intravital confocal fluorescence imaging and microcystoscopy in living animals with concomitant immunofluorescent staining of bladder tissues demonstrated that infused M-MSCs initially engrafted as multiple types of cells and gradually integrated as perivascular-like structure until 30 days after transplantation. Long-term engraftment ensured the efficient and long-lasting therapeutic effects of M-MSCs in ameliorating the defective bladder voiding function and repairing the pathological characteristics of IC/BPS bladder.

Thus, present study longitudinally monitors *in vivo* properties of the long-term grafted hESC derived M-MSCs in living animals as well as demonstrates their improved efficacy for

treating IC/BPS.

Keywords: Intravital imaging, Multipotent stem cells, Mesenchymal stem cell, Embryonic stem cell, Interstitial cystitis/Bladder pain syndrome.

CONTENTS

LIST OF FIGURES

LIST OF ABBREVIATIONS

BC: bladder capacity

BM: bone marrow

BP: bladder pressure

DAPI: 4',6-diamino-2-phenylindole

DAT: days after transplantation

GFP: green fluorescent protein

GRIN: gradient-index

hB2M: human β2 microglobin

HCl: hydrochloric acid

hESC: human embryonic stem cell

IAP: intra-abdominal pressure

IVP: intravesical pressure

IC/BPS: interstitial cystitis/bladder pain syndrome

LPS: lipopolysaccharide

MI: micturition interval

M-MSC: multipotent mesenchymal stem cell

MP: micturition pressure

MSC: mesenchymal stem cell

MV: micturition volume

NVC: non-voiding contraction

PBS: phosphate-buffered saline

PS: protamine sulfate

PSC: pluripotent stem cell

RQ-PCR: real-time quantitative PCR

RV: residual volume

SEM: standard error of the mean

Shh: sonic hedgehog

Smo: Smoothened

TUNEL: terminal deoxynucleotidyl transferase

dUTP nick-end labeling

UCB: umbilical cord blood

INTRODUCTION

Preclinical and clinical trials data suggest that mesenchymal stem cells (MSCs) may be considered as practical and safe sources of stem cells for the therapy of various human diseases [1-3]. MSCs are multipotent progenitor cells which may be isolated from a wide range of adult tissues such as bone-marrow (BM), adipose, peripheral blood, and dental pulp. MSCs may also be isolated from fetal tissues such as umbilical cord-blood (UCB), Wharton's jelly, placenta, and amniotic fluid [4, 5]. MSCs i) replace the damaged cells in the injured tissues, ii) exert the immunomodulatory functions, iii) also provide growth factors, mediate cell-cell interactions, and supply matrix proteins to modulate the microenvironment of damaged target tissues [6]. Based on these multiple beneficial properties, MSC-based therapy is rapidly finding potential applications in regenerative medicinal treatments for a range of intractable cardiovascular, musculoskeletal, neurological, and immunological disorders [1-3] as well as a number of bladder disorders [7].

Interstitial cystitis/bladder pain syndrome (IC/BPS) is among these bladder disorders which are likely amenable to stem cell therapy [8]. IC/BPS is a chronic inflammatory condition of the submucosal and muscular layers of the bladder [9]. IC/BPS patients suffer from vague pelvic pain that can be exacerbated by bladder filling and is often associated with urinary frequency, urinary urgency, and decreased quality of life. However, the causes of IC remain unknown and no effective treatments or cures have been developed [10]. Recently,

we have demonstrated that transplantation of MSCs derived from human UCB is an exciting therapeutic option for treating these intractable disorders [11, 12]. However, important questions remain about the functional integration of MSCs into existing tissue and the reasons for poor *in vivo* engraftment.

Importantly, the details of the therapeutic mechanisms remain controversial, and thus using MSC therapy as a standard therapy has been questionable. Recent studies have reported beneficial/therapeutic outcomes by so-called paracrine factors, growth factors, and cytokine which are secreted by transplanted stem cells, instead of direct replacement of the damaged tissues [13-15]. More importantly, direct analysis assessing biological and molecular properties of engrafted cells in pathological environment has not been considered in majority of current MSC therapy, thus their underlying therapeutic mechanisms, tumorigenic risk after transplantation and optimal transplantation protocols remain largely elusive. These critical limitations have hindered the development of effective and safe strategies for MSC-based therapies.

Intravital fluorescence microscopy enables the study of *in vivo* cellular processes such as cell trafficking, intercellular interaction, and vascular changes [16]. By utilizing a combination of high resolution confocal optical imaging system and endoscopic optical probes, dynamic changes of the infused stem cells may be repeatedly visualized at a single cell level in a longitudinal way. Recently, we showed that multipotent stem cells (M-MSCs) derived from human embryonic stem cells (hESCs) integrate long-term into bladder tissues

in a hydrochloric acid (HCl) instilled IC/BPS animal model representing an acute urothelial injury [17]. Importantly, we longitudinally monitored the *in vivo* distribution and properties of transplanted M-MSCs at single-cell resolution by intravital confocal imaging of bladder tissues in living animals over a period of six months.

In the present study, we have extended this novel imaging approach into a lipopolysaccharide (LPS) instillation IC/BPS rat model which represents more realistically represents chronic bladder injury to reveal the *in vivo* distribution of M-MSCs after transplantation into the IC/BPS bladder. We demonstrate implantation and migration and migration of M-MSCs from the serosa to the damaged urothelium by a novel combination of cystoscopy and intravital confocal imaging over a period of 40 days, and follow up with *ex vivo* imaging of immunostained tissue to demonstrate mechanisms for differentiation of the M-MSCs into epithelial, stromal, and endothelial cells, as well as functional integration of MSC into pre-existing perivascular cell clusters. Cystometric evaluation of bladder functions in non-anesthetized animals and related mechanistic studies demonstrated significant repair of chronically damaged bladder tissues with a single low-dose transplantation of M-MSCs, including classic measurements of IC/BPS markers such as non-voiding contraction, urothelium denudation, and mast cell infiltration in our LPS-IC rat group compared to a non-treatment group. The data presented expand on previous studies indicating that hESC derived M-MSCs are an ideal source for IC/BPS therapeutic options, ensuring a cost-effective supply of therapeutic cells with improved functional potency.

MATERIALS AND METHODS

Animal models and administration of M-MSCs

All animal experiments followed approval of the Institutional Animal Care and Use Committee of the University of Ulsan College of Medicine (IACUC-2016-12-088). The LPS-IC rat model was established by instillation of protamine sulfate (PS, 7 mg/rat, Sigma-Aldrich) to bladder of female 10-week-old Sprague-Dawley rats (OrientBio, Gapyong, Gyeonggi-do, Korea) via the urethra using a 26-gauge angiocatheter in order to make denudation in urothelium. After 45 minutes the bladders were emptied, washed with phosphate-buffer saline (PBS) solution and then given a second treatment with LPS (750 μg/rat, Sigma-Aldrich) for 30 minutes in order to induce inflammation. Weekly instillations of PS/LPS following this regimen over a period 5 weeks were used to induce a longer-lasting and possibly chronic injury to the urothelium. One week after final instillation of PS/LPS, low abdominal incision was made and the indicated dose of hESC-derived M-MSCs or PBS vehicle was directly injected into the outer layer of the anterior wall and dome of the bladder using a 500 μm syringe and a 26-gauge needle as previously reported [11, 12, 17, 18].

Culture of hESC-derived M-MSCs and establishment of GFP^+ M-MSCs

H9 hESCs were differentiated into M-MSCs as previously described [19, 20]. Established M-MSCs were cultured in EGM2-MV medium(Lonza, San Diego, CA, USA) on

plates coated with rat tail collagen type I (Sigma-Aldrich) in a humidified atmosphere containing 5% CO_2 at 37°C. Surface marker expression and multi-lineage differentiation of M-MSCs were characterized as previously described [17, 21]. All M-MSCs were expanded for fewer than ten passages to ensure they remained multipotent. To stably express GFP, M-MSCs were infected with a GFP-expressing lentivirus, which was generated as previously described [21]. In brief, GFP was sub-cloned into the pENTR4 entry vector (Invitrogen, Carlsbad, CA, USA) and then transferred to the pLenti6.2/V5-DEST lentiviral vector (Invitrogen) using Gateway® Technology (Invitrogen). Lentivirus was produced using a four-plasmid transfection system (Invitrogen). Two days after transfection of the 293 FT packaging cell line, supernatants containing recombinant pseudo-lentiviral particles were collected and concentrated by precipitation using a Lenti-X Concentrator kit (Clontech, Mountain View, CA, USA). M-MSCs were infected with the concentrated virus using 6 μg/mL polybrene (Invitrogen), and infected cells were selected using 6 μg/mL blasticidin (Invitrogen). Stable expression of GFP was examined using a BDFACS Canto II flow cytometer (BD Biosciences, Mountain View, CA, USA) and an inverted fluorescence microscope (EVOS FL Color Imaging System, Life Technologies, Carlsbad, CA, USA).

Longitudinal in vivo confocal imaging using μ-endoscopy and microscopy

A total of 1×10^6 GFP^+ M-MSCs were injected into the bladder serosa of LPS-IC rats, following acquisition of baseline images (**Figure 7B**). Confocal microscopy and imaging with a micro-endoscopic optical probe were performed in living animals before

transplantation and for up to 6 months post-transplantation. For confocal microscopy, a 5 mm incision was made in the abdomen and widened to expose the bladder and allow imaging using a 40× objective lenses. The microscope was aligned such that the site of injection was centered, with deviations of less than 1 mm. The excitation laser was focused on the outer layer of the bladder, and then the point of focus was adjusted inward to attain consistent and meaningful image depths. For cystoscopy, a micro-endoscope with a diameter of 1.2 mm and a length of 5.5 cm was fabricated by cementing three GRIN lenses together in a rigid tube suitable for front-view image transfer [16]. The transverse and lateral resolutions were 1 and 11 μm in the air, respectively, which was sufficient to monitor M-MSCs at single-cell resolution in the bladder mucosa. A custom-built system with three axes of translational freedom was used to mount and align the probe consistently in the confocal microscope, and the probe was inserted via the urethra and positioned close to the pelvis. Care was taken to ensure that the procedure and alignment were performed consistently, resulting in deviations of less than 0.5 mm. Focus was attained by abutting the GRIN probe to the inner bladder wall and adjusting the point of focus inward using the microscopy platform. GFP was excited using a continuous 488 nm laser diode and was scanned along the objective and endoscope tip at a rate of 30 fps using a scanning galvanometric system. Photomultiplicative detectors were used in tandem with dichroic filters to capture emitted fluorescence while avoiding noise caused by the excitation laser and autofluorescence.

Unanesthetized and unrestrained cystometrogram (awake cystometry)

Cystometric evaluation was performed in the awake state with unrestrained animals in metabolic cages. Three days prior to the cystometrogram, intravesical pressure (IVP) and intra-abdominal pressure (IAP) recordings were performed, as described previously [22, 23]. The urethra was approached by using a PE-50 catheter (Clay Adams, Parsippany, NJ) connected to a pressure transducer (Research Grade Blood Pressure Transducer; Harvard Apparatus, Holliston, MA, USA) and a microinjection pump (PHD22/2000 pump; Harvard Apparatus). The voiding volumes were recorded by means of a fluid collector connected to a force displacement transducer (Research Grade Isometric Transducer; Harvard Apparatus) as normal saline was infused into the bladder at a rate of 0.4 ml/min. The IVP, IAP and voiding volumes were recorded continuously using Acq Knowledge 3.8.1 software and an MP150 data acquisition system (Biopac Systems, Goleta, CA, USA) at a sampling rate of 50 Hz. The mean values from three reproducible voiding cycles using individual animals were used for evaluation. Criteria for counting non-voiding contraction (NVC) was when the increments of IVP exceeded 15 cmH_2O from baseline without expelled urine. BP was defined as the lowest bladder pressure during filling, MP as the maximum bladder pressure during the micturition cycle, MV as the urine volume of expelled urine, and RV as the urine volume remaining following voiding. In agreement with prior work, MI was defined as the interval between micturition contractions and BC was defined as MV + RV. The mean values from three reproducible micturition cycles using five individual animals (n=5) were used for evaluation.

Histological and gene expression analyses

The histological analysis quantification of epithelial denudation, mast-cell infiltration, tissue fibrosis, and apoptosis were assessed by immunostaining of cytokeratin, Toluidine blue staining (8544-4125; Daejung Chemicals & Metals, Seoul, Korea), Masson's trichrome staining (Junsei Chemical, Tokyo, Japan), and TUNEL staining (1 684 795; Roche, Mannheim, Germany), respectively as previously described [11, 12, 17]. Injected GFP^+ M-MSCs in the bladder were tracked by immunofluorescent staining with specific rabbit polyclonal antibody (ab290; Abcam, Cambridge, MA). GFP^+ cell epithelial, stromal, and endothelial characteristics were further examined by staining with antibodies against E-cadherin (612130; Clone 36; FITC-conjugated, BD Biosciences, San Diego, CA), vimentin (sc-6260; Santa Cruz Biotechnology), and CD31 (sc-376764; Santa Cruz Biotechnology) respectively. Determination of WNT activation was by β-catenin immunofluorescence staining (sc-7199; Santa Cruz Biotechnology). Alexa 488 (A11001)- or 564 (A11010)-conjugated anti-mouse or -rabbit antibodies (Molecular Probes, Grand Island, NY, USA) were used for immunostaining images, and nuclei were counterstained with 4´ ,6-diamino-2-phenylindole (D9542; DAPI, Sigma-Aldrich). Three randomly chosen representative areas were selected from each slide for quantitative digital image analysis using Image Pro 5.0 software (Media-Cybernetics, Rockville, MD, USA).

For gene expression analysis, preparation of total RNA, reverse transcription, and quantification of the indicated transcripts were performed using an RNeasy Mini Kit (Qiagen

Inc., Valencia, CA), TaqMan Reverse Transcription Reagents (Applied Biosystems), and real-time quantitative PCR (RQ-PCR) with the PikoReal™ Real-Time PCR System (Thermo Scientific) with iQ™ SYBR Green PCR Master Mix (Bio-Rad, Hercules, CA), as described previously [24, 25]. Three randomly chosen areas from each slide (n=15) or duplicated RQ-PCR assays (n=10) using five independent animals were used to quantify the digital image or gene expression data.

Statistical analysis

Data are reported as the mean ± standard error of the mean (SEM) and were analyzed by GraphPad Prism 6.0 software (GraphPad Software, La Jolla, CA). Differences and significance were verified by one-way or two-way ANOVA followed by Bonferroni post hoc tests. A p-value less than 0.05 was considered statistically significant.

RESULTS

Intravital confocal and endoscopic imaging of transplanted M-MSCs in an animal model of IC/BPS

The unlimited proliferation capacity and pluripotency of hESCs may enable production of a large number of high-quality therapeutic cells by well-controlled differentiation *in vitro* and they exhibit improved survival, engraftment, and functionality *in vivo* [19]. We previously reported that hESC-derived M-MSCs remain engrafted in an HCl instillation-induced animal model of IC/BPS until 6 months post-transplantation [17]. However, this model, in which acute pathology is induced by a supra-physiological insult, does not accurately reflect the chronic nature of IC/BPS and consequently, its clinical relevance is limited. Here, we used an endotoxin instillation-induced model of chronic bladder pain. Protamine sulfate (PS) and LPS were instilled into the bladders of rats weekly for 5 weeks to induce longer-lasting and chronic urothelial injury, which accurately mimics the chronic and inflammatory nature of IC/BPS [26, 27]. We transplanted the same lot of hESC-derived M-MSCs as was previously transplanted into our acute IC/BPS animal model [17]. In line with this previous report, these cells exhibited several typical features of MSCs, including a spindle- and fibroblast-like morphology (**Figure 1A**) and positive surface expression of markers of MSCs (CD44, CD73, and CD105) and pericytes (CD146 and NG2) (**Figure 1B**). One week after the final instillation, 1×10^6 M-MSCs expressing green fluorescent protein (GFP) were injected

directly through the outer layer of the bladder into the area between the muscle and serosa (**Figure 2A**). Lentiviral delivery of a GFP-expressing cassette ensured that the majority of M-MSCs stably expressed GFP during long-term maintenance for up to 5 weeks (**Figure 3A, 3B**) and upon multi-lineage (adipogenic, osteogenic, and chondrogenic) differentiation (**Figure 3C**).

Next, we investigated the properties of engrafted M-MSCs in living animals. To this end, we performed confocal imaging of the outer layers of the bladder close to the injection site by making a small incision in the abdomen (**Figure 2B, 2C**). Meanwhile, we imaged the bladder interior using miniaturized front-view gradient-index (GRIN) endoscopic optical probes, which allowed non-invasive monitoring of the integration of transplanted M-MSCs into the damaged urothelium (**Figure 2B, 2C**). Fluorescence micro-endoscopy of the urothelium and confocal microscopy of the serosa are shown in **Figure 4** and **Figure 6**, respectively. Intense focal fluorescence was detected in the urothelium by endoscopy at 3 days after transplantation (DAT) (**Figure 4**). The fluorescence intensity decreased until 7 DAT, did not change until 14 DAT, increased until 21 DAT, and started to decrease again at around 30 DAT (**Figure 5**). The focus of the images improved over the first 7 DAT and progressively worsened from 30 DAT, indicating that M-MSCs migrated away from the focal plane of the probes. The focal depth of GRIN fluorescence endomicroscopy probes is 20–40 μm in tissues. Therefore, these observations provide physical evidence of cell migration from the serosa and muscularis to the urothelium, followed by cell migration to the lamina

propria and differentiation.

Intravital confocal imaging of the outer layers of the bladder yielded similar findings. The fluorescence intensity decreased rapidly until 7 DAT and gradually until 42 DAT (**Figure 6**). The GFP^+ cells had multiple shapes and were distributed throughout the entire bladder at 3 DAT. GFP fluorescence at 3 DAT, which labeled cells with multiple shapes and was broadly distributed across the entire bladder, was observed in both endoscopy (**Figure 4**) and confocal micrographs (**Figure 6A, 6B**). As the fluorescence intensity decreased from 7 DAT (**Figure 6C**), engrafted GFP^+ cells came into focus and the majority were located in blood vessel-like structures in confocal micrographs (**Figure 6A, 6B**). Negligible baseline fluorescence or autofluorescence was detected in animals not injected with GFP^+ M-MSCs (**Figure 7A, 7B**). Little GFP fluorescence with clear cellular morphology was observed at 42 DAT.

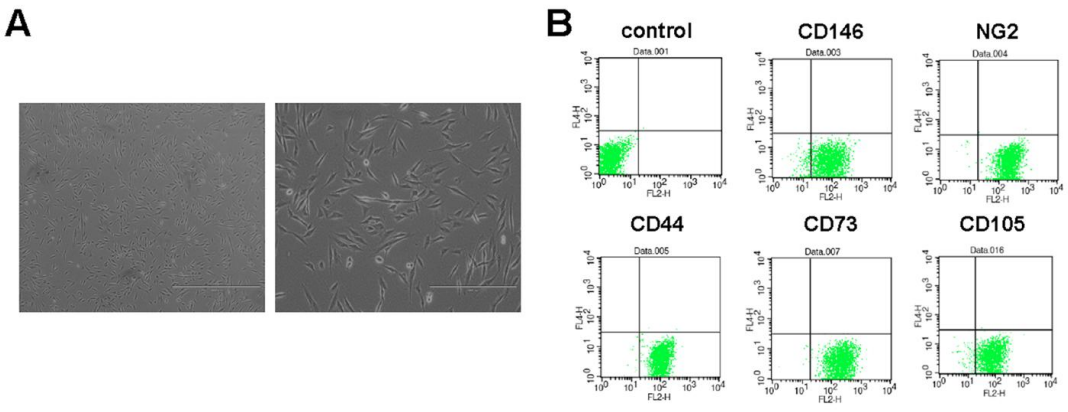

Figure 1. Characterization of hESC-derived M-MSCs.

(A) Morphological characterization of M-MSCs (left panel; magnification ×40, scale bar = 400 μm and right panel; magnification ×100, scale bar = 1,000 μm). **(B)** Analysis of surface antigen expression showing that M-MSCs were positive for markers of MSCs (CD44, CD73, and CD105) and pericytes (CD146 and NG2).

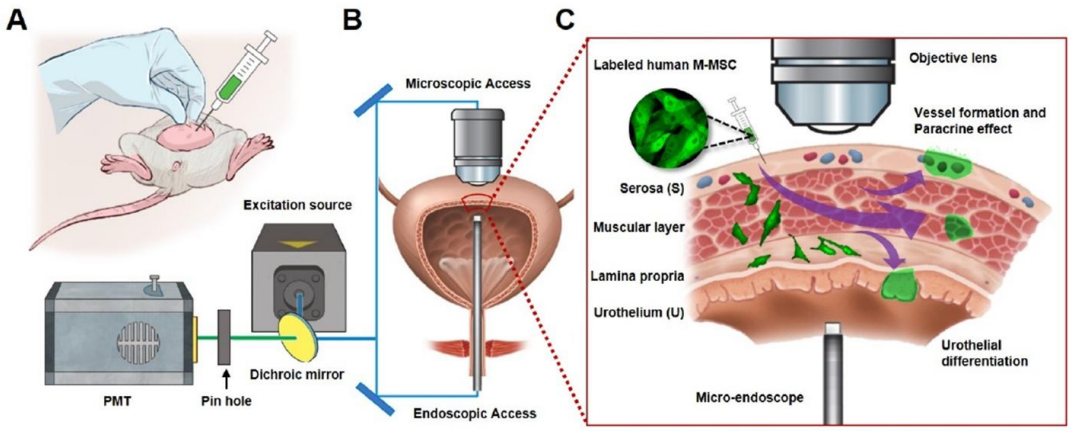

Figure 2. Longitudinal imaging of transplanted M-MSCs in living animals.

(A) Schematic diagram of the injection of hESC-derived M-MSCs into the bladder wall of IC/BPS rats. **(B)** Schematic diagram of confocal imaging of the external bladder wall and micro-endoscopy of the internal bladder wall to monitor the distribution, migration, and integration of transplanted M-MSCs. The objective lens was inserted through a small incision in the overlying abdomen to image the outer layer of the bladder. The front-view GRIN micro-endoscope probe was inserted into the bladder of an anesthetized rat on an XYZ stage to image the surface of the urothelium. **(C)** Schematic diagram of the migration of M-MSCs from the serosa, where they were injected, to the lamina propria and urothelium. M-MSCs initially differentiate in the urothelium and thereby repair the denuded urothelial wall, and later integrate into blood vessel-like structures. The injection site of M-MSCs and the viewpoints are indicated.

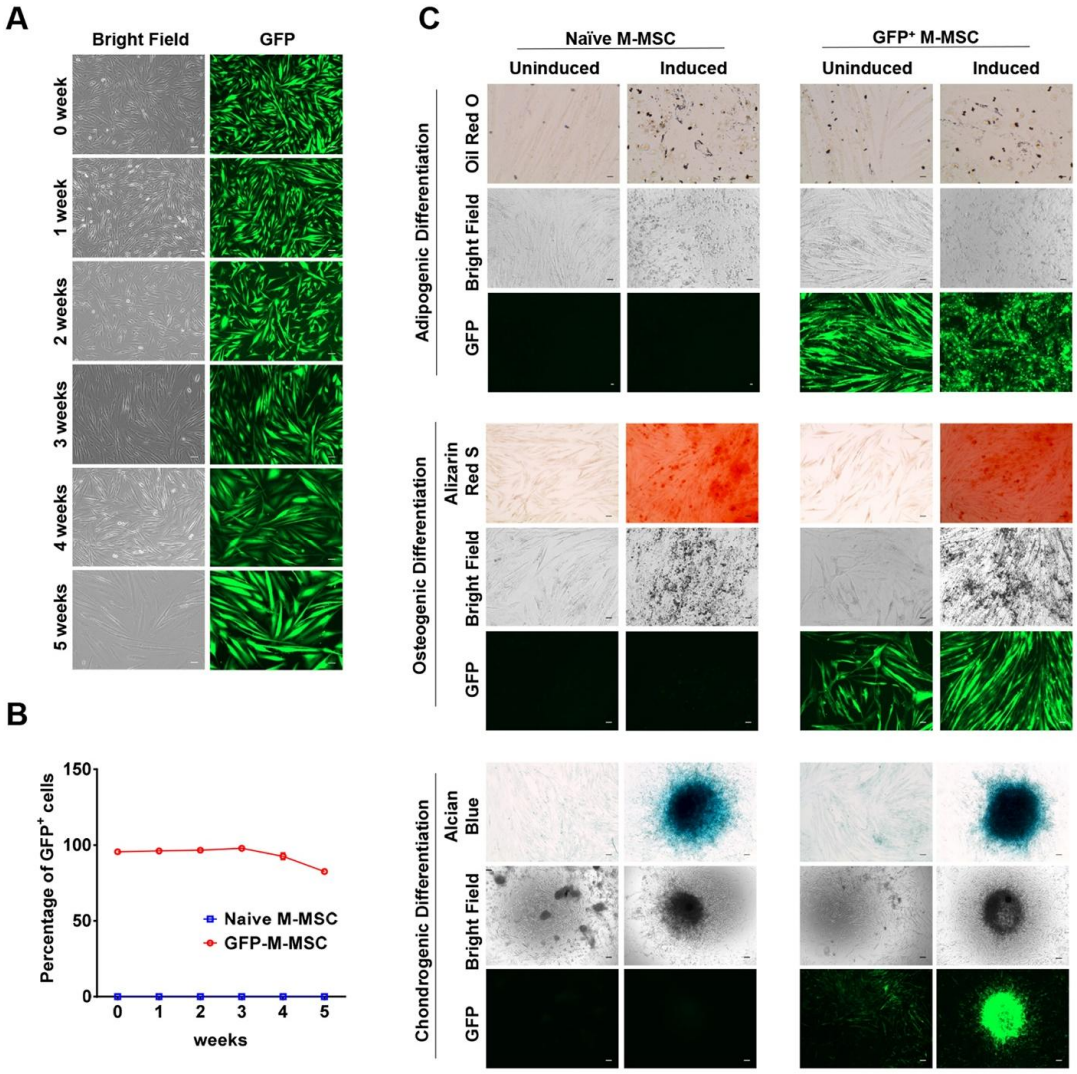

Figure 3. Stable expression of GFP in GFP$^+$ M-MSCs.

Expression of GFP in M-MSCs infected with a lentivirus containing a GFP-expressing cassette during long-term cultivation and multi-lineage differentiation. **(A and B)** Expression of GFP during cultivation of GFP$^+$ M-MSCs for 5 weeks was monitored using an inverted fluorescence microscope (**A**; magnification ×100, scale bar = 100 μm) and by FACS analysis **(B)**. **(B)** The percentage of GFP-expressing cells determined by FACS analysis was

quantified from three independent experiments. Data are presented as the mean ± SEM. **(C)** Expression of GFP during adipogenic (upper panel; ×200 magnification; scale bar = 20 μm), osteogenic (middle panel; ×200 magnification; scale bar = 40 μm), and chondrogenic (lower panel; ×40 magnification; scale bar = 200 μm) differentiation in control (Naïve) and GFP-expressing M-MSCs (GFP^+ M-MSCs). Adipogenic, osteogenic, and chondrogenic differentiation was characterized by Oil Red O, Alizarin Red S, and Alcian Blue staining, respectively.

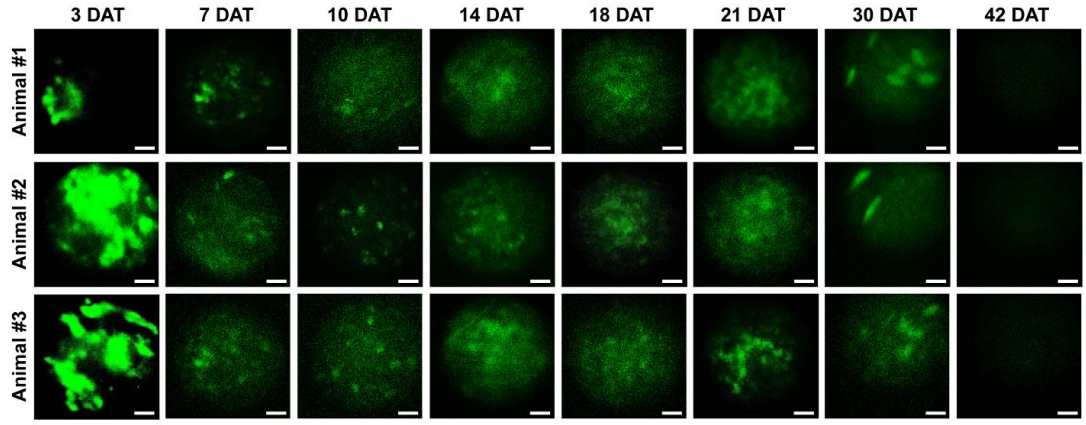

Figure 4. Longitudinal microcystoscopy of transplanted M-MSCs in living animals.

Time-lapse micro-endoscopy imaging of engrafted M-MSCs in the bladders of LPS-IC rats (three independent animals) at 3–42 days after transplantation (DAT). Endoscopic images obtained using a GRIN optical probe (magnification ×40, scale bar = 50 μm). Quantitative data of intravital micro-endoscopic imaging is presented in **Figure S3**.

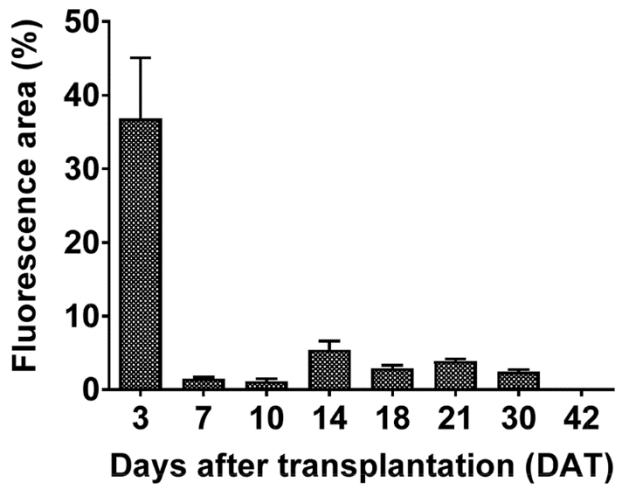

Figure 5. Quantitative assay of intravital micro-endoscopic imaging

Percentage of the fluorescent area in confocal endoscopic micrographs.

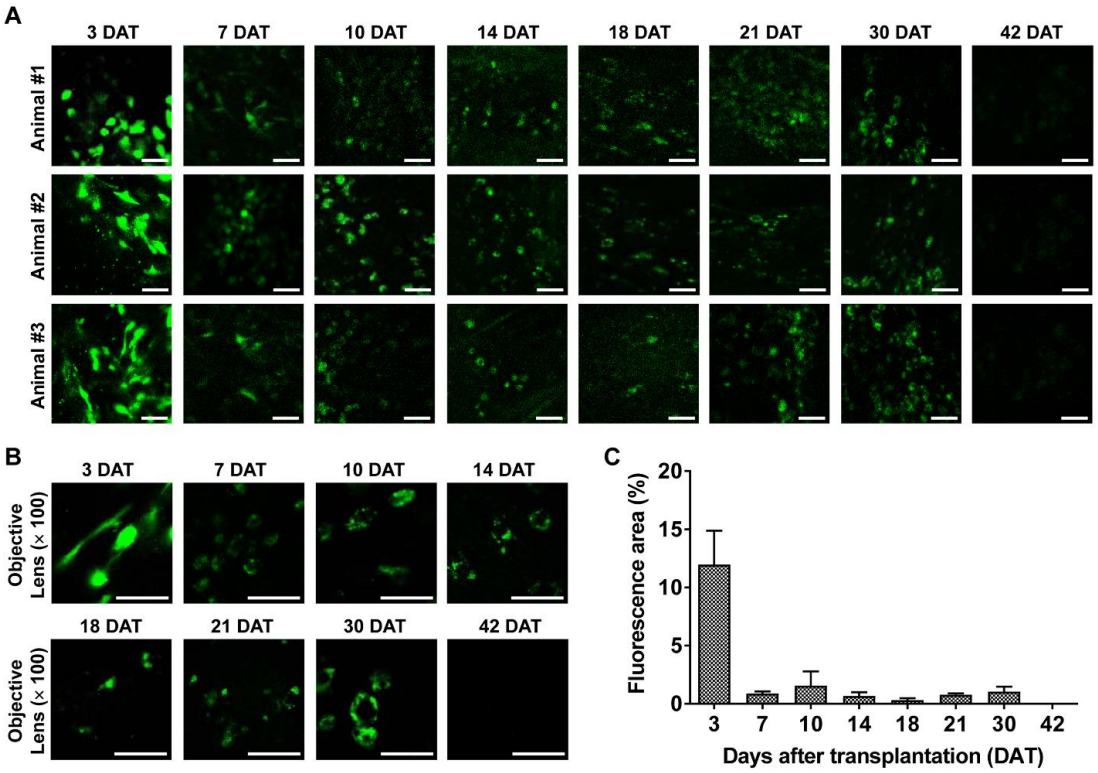

Figure 6. Longitudinal confocal microscopy of transplanted M-MSCs in living animals.

Time-lapse confocal microscopy of engrafted M-MSCs in the bladders of LPS-IC rats (three independent animals) at 3–42 days after transplantation (DAT). **(A and B)** Confocal micrographs obtained using an objective lens (**A**; magnification ×40, scale bar = 50 μm and **B**; ×100, scale bar = 50 μm). The majority of transplanted M-MSCs at 30 DAT were detected in a vascular-like structure located close to the outer layer of the bladder. **(C)** Percentage of the fluorescent area in confocal micrographs.

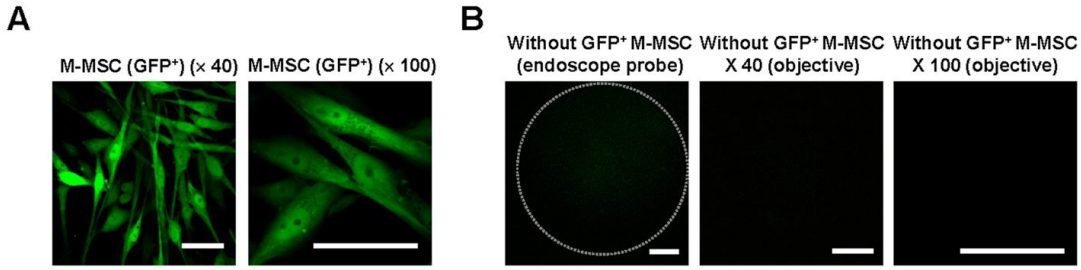

Figure 7. Low level of autofluorescence in intravital imaging.

(A) Representative images of GFP in cultured GFP^+ M-MSCs (magnification ×40 and ×100).

(B) Longitudinal imaging of living animals not transplanted with GFP^+ M-MSCs. Time-lapse images of the bladders of LPS-IC rats were obtained using a front-view GRIN optical probe endoscopically inserted into the bladder (left, magnification ×40) or an objective lens (middle; magnification ×40, right; magnification ×100). Baseline images from rats not injected with GFP^+ M-MSCs show low autofluorescence, and weak fluorescence signals overall are detected by intravital imaging. Scale bar = 50 μm.

Immunostaining of the cellular features of the infused M-MSCs in LPS IC/BPS model

Exposure to dramatic environmental changes or adverse microenvironments in damaged tissues may induce apoptosis of transplanted MSCs and impair their engraftment. Terminal deoxynucleotidyl transferase dUTP nick-end labeling (TUNEL) of bladder tissues indicated that apoptosis of transplanted GFP^+ M-MSCs was highest at 3 DAT, at which point ~20% of these cells were apoptotic (**Figure 8**). The percentage of transplanted cells that were apoptotic was reduced to less than 10% at 7 DAT, and almost none of these cells were apoptotic at 30 DAT. These findings indicate that apoptosis also contributes to the rapid decline in GFP fluorescence up to 3 DAT in both endoscopy (**Figure 4**) and confocal micrographs (**Figure 6**).

Next, to analyze the cellular properties of surviving M-MSCs, immunohistological analysis of bladder tissues was performed by multichannel scanning laser confocal imaging. Engrafted cells, epithelial cells, stromal cells, and endothelial cells were detected based on expression of GFP, E-cadherin, vimentin, and CD31, respectively (**Figure 9, Figure 10,** and **Figure 11**). At 7 DAT, many GFP^+ cells were detected in the urothelium, lamina propria, and serosa. The majority of these cells were located between the serosa and muscular layer, where they had been injected, and a few were found in the muscular layer. All GFP^+ cells in the urothelium were E-$cadherin^+$, indicating that they had differentiated into epithelial cells (**Figure 9A, top row**). The majority of GFP^+ cells located between the serosa and muscularis were strongly stained with an anti-vimentin antibody, indicating that they had differentiated

into stromal cells (**Figure 9A, second row**) and perivascular cells (**Figure 9A, third row**). GFP^+ cells located in the endothelium were $CD31^+$, indicating that they had differentiated into endothelial cells (**Figure 9A, fourth row**). Non-specific staining in immunofluorescence assays was ruled out by two negative controls: i) co-staining with mouse and rabbit IgG control antibodies instead of primary antibodies, and ii) co-staining of bladder sections from animals not injected with GFP^+ M-MSCs (**Figure 10A**). Taken together, these results demonstrate that transplanted M-MSCs stably engrafted and migrated to the damaged urothelium, where they differentiated into multiple cell types.

Consistent with the intravital imaging, GFP^+ cells in the urothelium were rarely observed from 30 DAT and mainly localized in the serosa (**Figure 9B**). During this period, engrafted cells formed discrete foci and the majority were detected in blood vessel-like structures. Confocal imaging of bladder tissues indicated that engrafted M-MSCs had differentiated into $CD31^+$ endothelial cells as well as $vimentin^+$ or α-smooth muscle actin $(SMA)^+$ perivascular cells close to blood vessels at 30 DAT (**Figure 9B** and **Figure 10B**). The differentiation of transplanted cells into perivascular cells was further evaluated by investigating cells that co-expressed vimentin and human β2 microglobin (hB2M) in blood vessel-like structures (**Figure S7**). However, no such cells were observed at 42 DAT (**Figure 12**). In summary, by performing a combination of intravital imaging and immunohistological analysis, we monitored and characterized M-MSCs engrafted in the bladder of a rat model of IC/BPS as they initially replenished the urothelial layer and progressively differentiated into

perivascular cells.

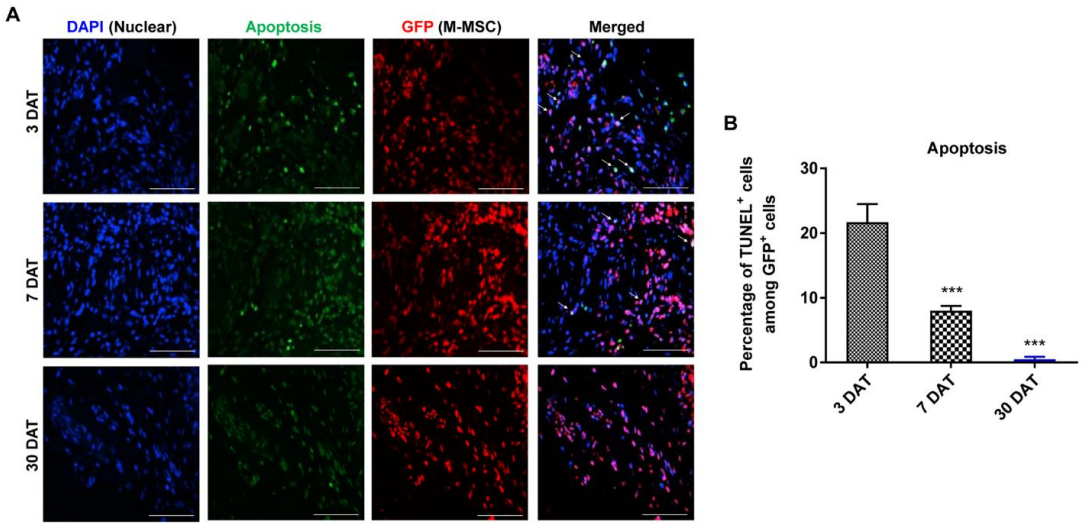

Figure 8. Apoptosis of transplanted M-MSCs.

(A) Representative images of staining to detect TUNEL$^+$ apoptotic cells (red) among transplanted GFP$^+$ M-MSCs (green) (magnification ×400, scale bar = 20 μm) in bladder tissues of LPS-IC + M-MSC rats at the indicated number of DAT. **(B)** Quantification of the staining results. Data show the percentage of GFP$^+$ cells that were TUNEL$^+$ (n = 8) and are presented as the mean ± SEM. ***p<0.001 compared with the 3 DAT group according to a one-way ANOVA with the Bonferroni post-hoc test.

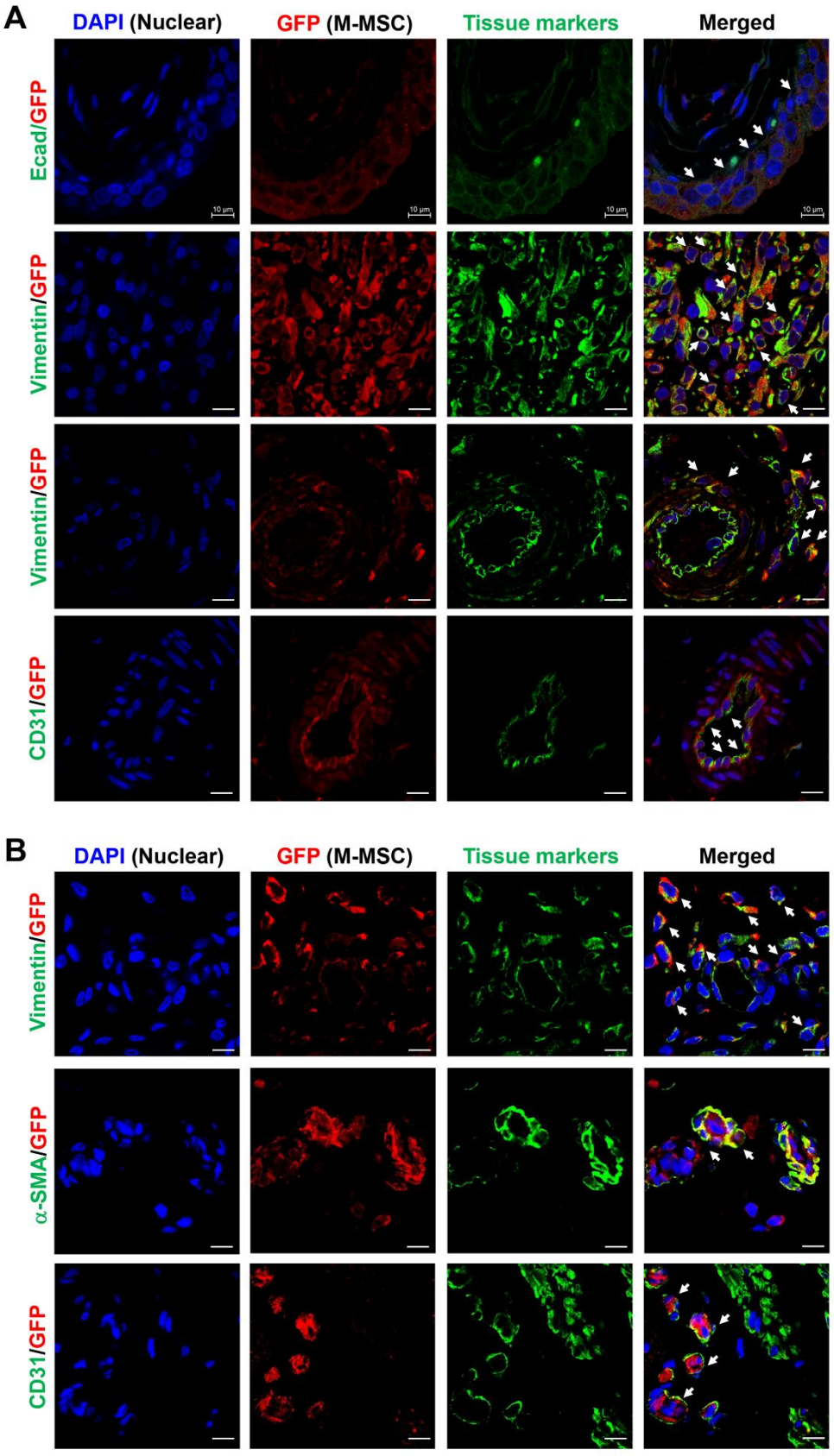
A
DAPI (Nuclear)
GFP (M-MSC)
Tissue markers
Merged
Ecad/GFP
Vimentin/GFP
Vimentin/GFP
CD31/GFP
10 μm
B
DAPI (Nuclear)
GFP (M-MSC)
Tissue markers
Merged
Vimentin/GFP
α-SMA/GFP
CD31/GFP

Figure 9. Immunostaining analysis of transplanted M-MSCs.

Confocal micrographs of M-MSCs stably expressing GFP (red) and immunostaining o f the marker proteins E-cadherin (Ecad), vimentin, α-SMA, and CD31 (green) in blad der sections of LPS-IC + M-MSC rats at 7 DAT **(A)** and 30 DAT **(B)** (magnification ×1,000, scale bar = 10 μm). Nuclei were stained with DAPI (blue). Arrows indicate GFP^+ engrafted cells co-expressing each tissue marker. Notably, the majority of trans planted GFP^+ cells at 7 DAT was strongly stained with the vimentin expressing stro mal cells (**second row in A**) and perivascular cells (**third row in A**).

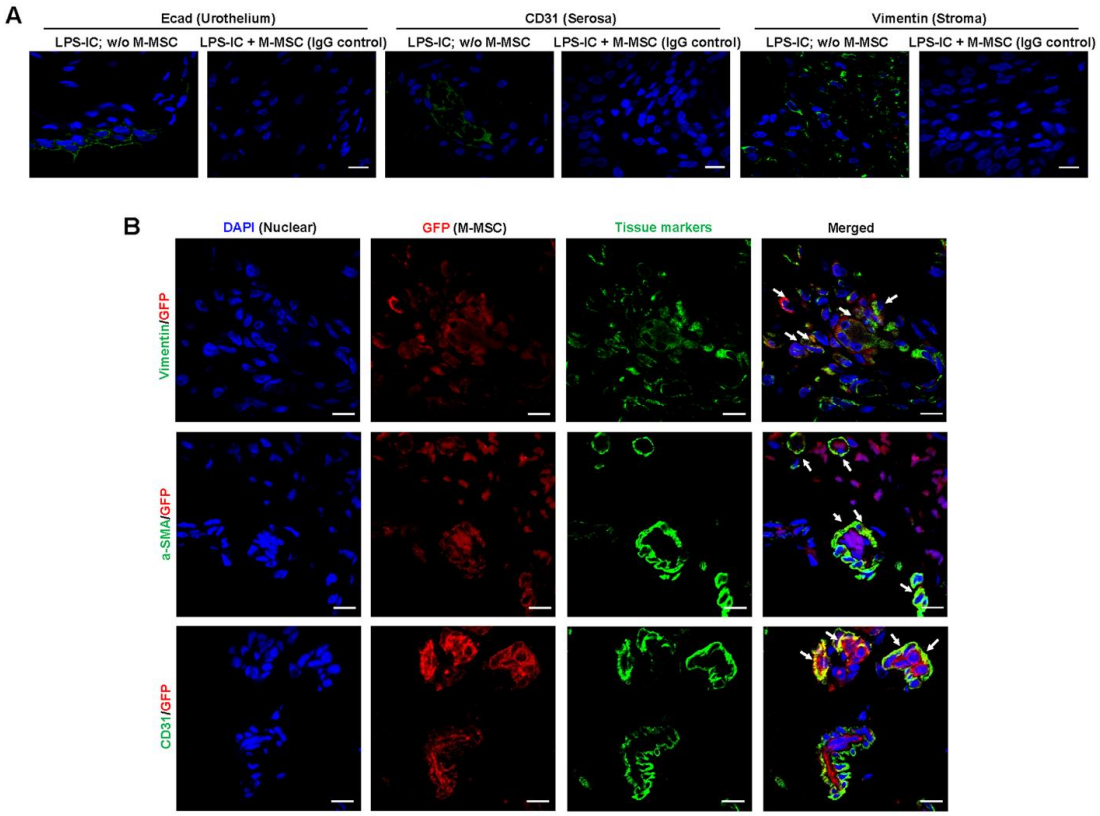

Figure 10. Immunostaining of transplanted M-MSCs.

(A) To rule out the possibility of non-specific staining, bladder tissues of LPS-IC + M-MSC rats were co-stained with mouse and rabbit IgG control antibodies, and bladder tissues of LPS-IC rats not injected with M-MSCs (LPS-IC; w/o M-MSC) were co-stained for the indicated markers (green) and GFP (red) (magnification ×1,000, scale bar = 10 μm) as two sets of negative controls. **(B)** Representative confocal micrographs of bladder sections of LPS-IC + M-MSC rats stained for GFP (red) and vimentin, α-SMA, or CD31 (green) at 30 DAT (magnification ×1,000, scale bar = 10 μm). Nuclei were stained with DAPI (blue).

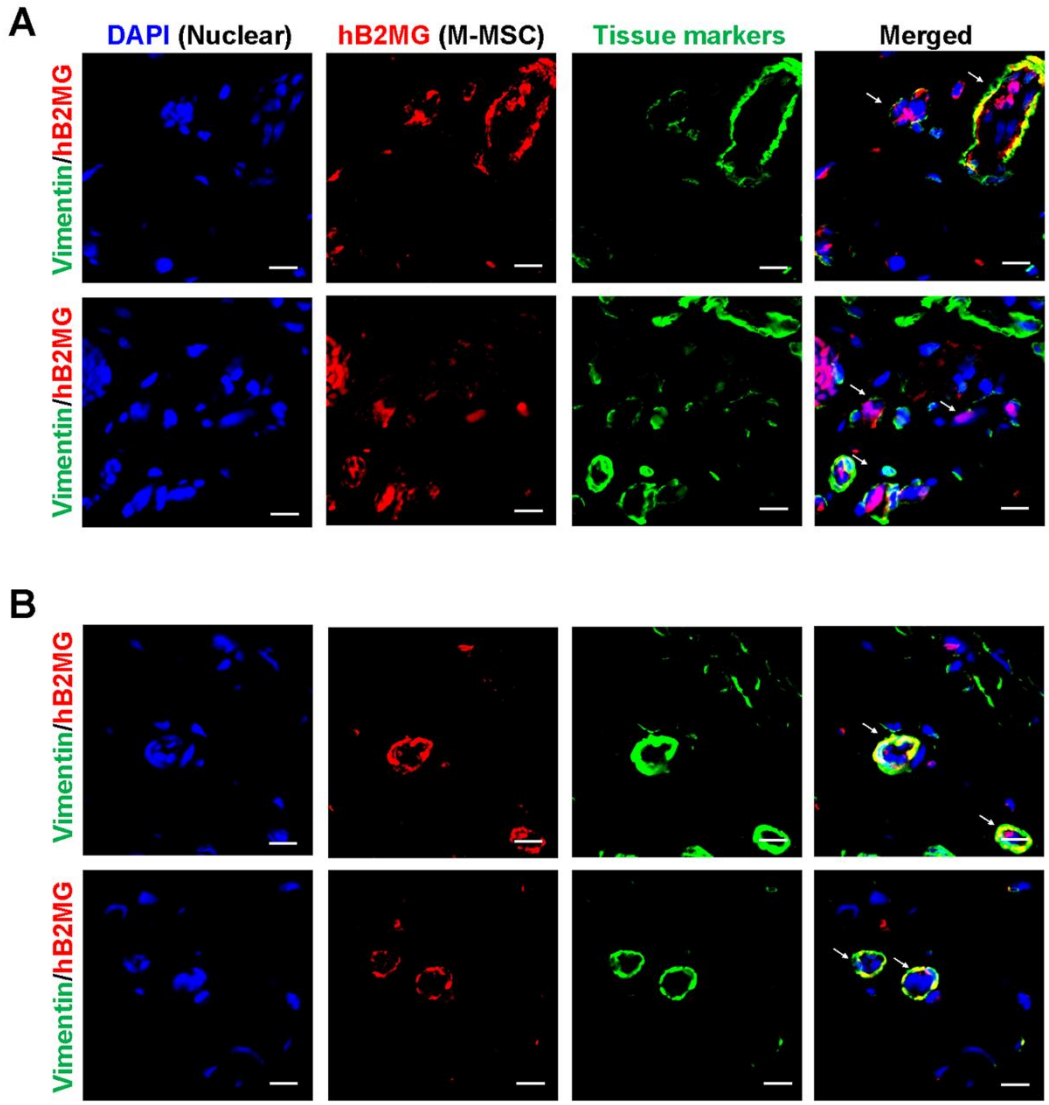

Figure 11. Co-expression of vimentin and human antigens in transplanted M-MSCs.

Representative confocal micrographs of bladder sections of LPS-IC + M-MSC rats stained for hB2M (red) and vimentin at 7 DAT (upper panel) and 30 DAT (lower panel) in blood vessel-like structures (magnification ×1,000, scale bar = 10 μm). Nuclei were stained with DAPI (blue).

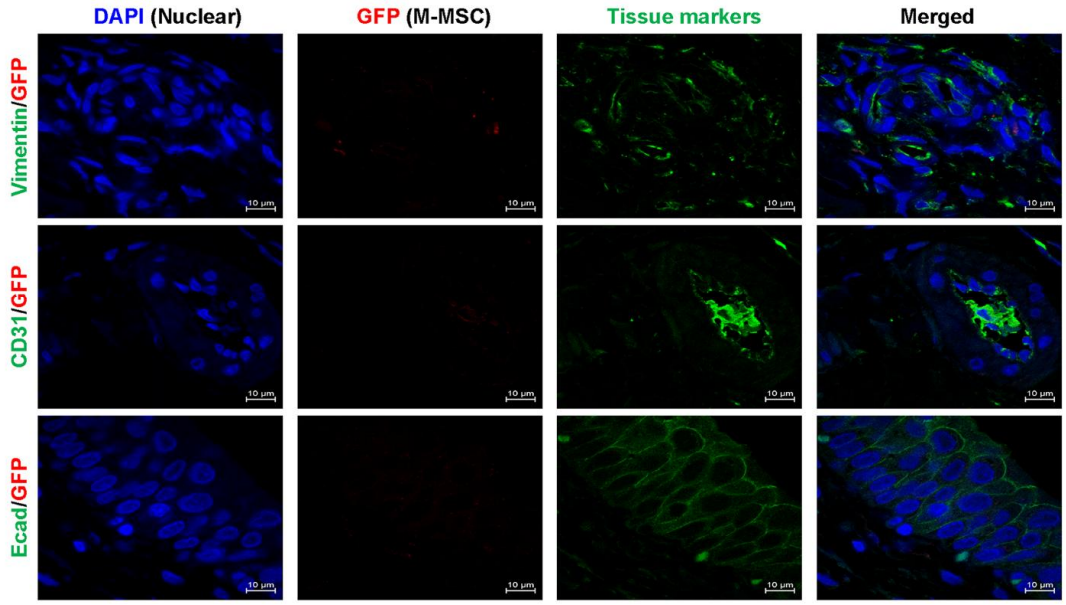

Figure 12. Disappearance of transplanted M-MSCs at 1 month after transplantation.

Representative confocal micrographs of bladder sections of LPS-IC + M-MSC rats stained for GFP (red) and vimentin, E-cadherin (Ecad), or CD31 (green) at 42 DAT (magnification ×1,000, scale bar = 10 μm). Nuclei were stained with DAPI (blue).

Evaluating in vivo therapeutic potency of M-MSC for treating IC/BPS

Given confirmation of long-term engraftment of more than 1 month, we next evaluated the *in vivo* efficacy of M-MSC therapy by a single administration of 1×10^6 M-MSC directly into the bladders of LPS-IC animals. To precisely investigate functional improvement, we employed awake filling cystometry which allows for long term evaluation of bladder function in freely moving animals (**Figure 13A, 13B**). In comparison with animals in a sham-operated group (sham), rats subject to IC/BPS due to induced LPS instillation (LPS-IC group) exhibited irregular voiding patterns and decreased micturition intervals (MI) (27.42±0.55 vs. 98.29±1.56 sec; $p<0.001$), micturition volume (MV) (0.15±0.01 vs. 0.35±0.02 mL; $p<0.001$), bladder capacity (BC) (0.18±0.00 vs. 0.66±0.01 mL; $p<0.001$), and residual volume (RV) (0.03±0.01 vs. 0.31±0.02 mL; $p<0.005$) (**Figure 13B, 13C**). Animals in the LPS-IC group showed increased micturition pressure (MP) (95.86±1.45 vs. 53.29±0.45 mL; $p<0.001$), basal bladder pressure (BP) (60.95±4.12 vs. 31±2.3 cmH_2O; $p<0.01$), and maximum pressure (97.17±1.45 vs. 53.43±0.45 cmH_2O; $p<0.001$).

A single transplantation of 1×10^6 M-MSCs into the LPS-IC + M-MSC group significantly ameliorated these defective voiding parameters (**Figure 13B, 13C**). Beneficial effects were also observed for low-dosage treatments by administration of more than 2.5×10^5 M-MSCs (**Figure 13B, 13C**). In particular, animals in the LPS-IC group characteristically showed an increased frequency of contraction during the non-voiding period (non-voiding contraction, NVC) even with low dosage M-MSC therapies.

In line with awake cystometry data, administration of more than 2.5×10^5 M-MSCs

restored histological alterations such as the severe denudation of urothelium, mast cell infiltration, and apoptosis (**Figure 14A, 14B**). However, little tissue fibrosis was detected in the bladders of LPS-IC group rats at these lower dosages.

Next, we examined whether the LPS-IC animals could exhibit chronic symptoms like IC/BPS patients. These animals exhibited defective bladder voiding functions which were sustained for 4 weeks after the final LPS instillation (**Figure 15A** and **Figure 16**). Accordingly, increased urothelial denudation, inflammation, mast cell infiltration, and apoptosis, which are characteristics of the bladders of IC/BPS patients [28-31], were sustained for more than 4 weeks in the bladder tissues of LPS-IC animals (**Figure 15B, 15C,** and **Figure 17**). Importantly, the therapeutic effects of a single administration of M-MSCs regarding bladder voiding functions and histological injuries were sustained for a long-term of two to four weeks following transplantation (**Figure 15**). In particular, normal NVC, the most common factor for evaluating bladder voiding function in clinical care, was observed for 4 weeks in the LPS-IC animals transplanted with M-MSCs (**Figure 14**). Therefore, this preclinical study demonstrated that M-MSC therapies provide effective and long-lasting therapeutic outcomes to repair the voiding functions and abnormal histological damage observed in LPS-IC bladder patients, while protecting from further tissue damage.

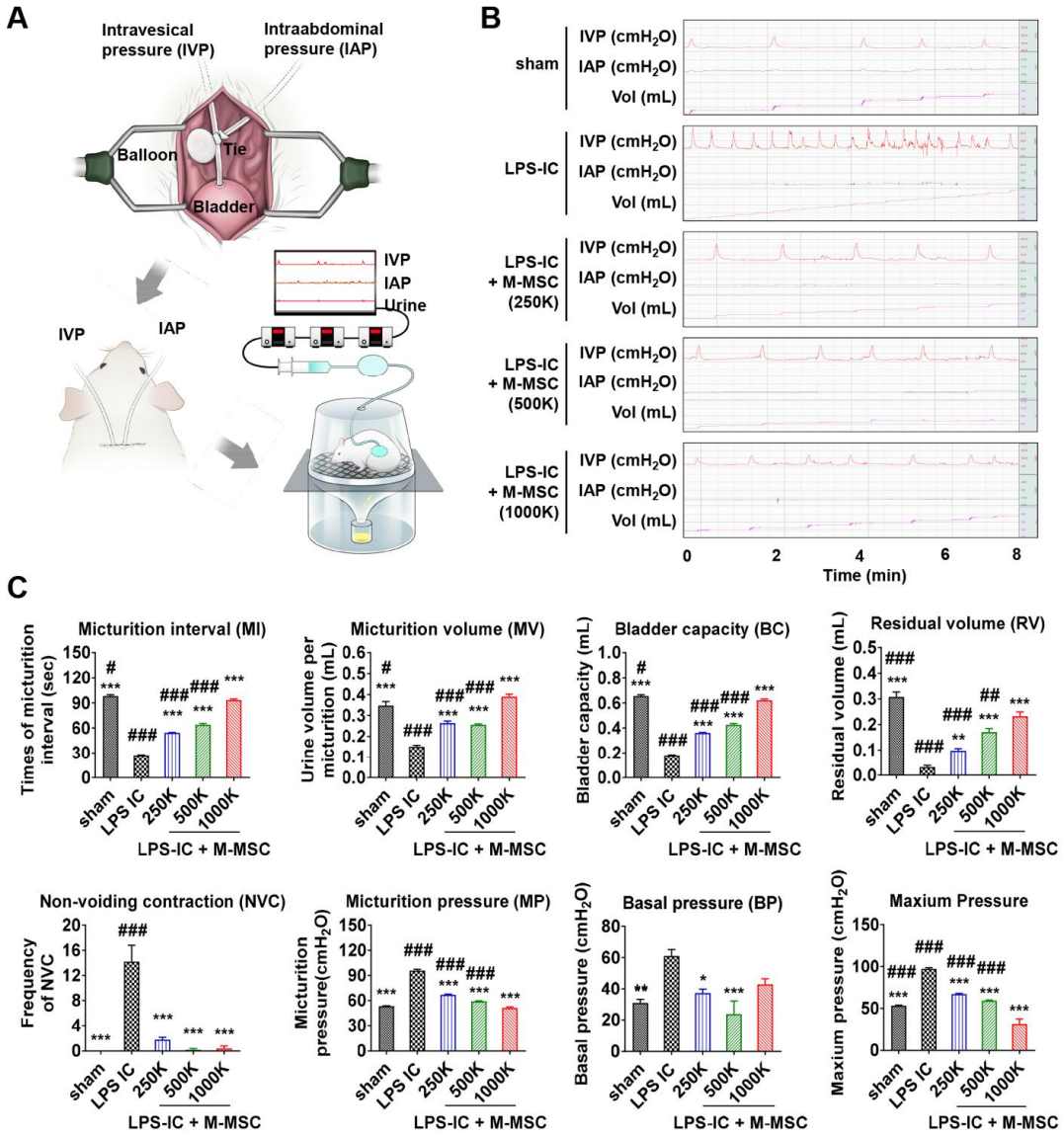

Figure 13. Injection of M-MSCs ameliorates bladder voiding functions in LPS-IC rats.

(A) Schematic diagram of awake cystometry. **(B and C)** Representative awake cystometry results **(B)** and quantitative bladder voiding data **(C)** at 1 week after injection of LPS-IC rats with the indicated number of M-MSCs (K = thousand). Data are presented as the mean ± SEM (five independent animals per group). *p<0.05, **p<0.01, and *** p<0.001 compared

with the LPS-IC group; #p<0.05, ##p<0.001, and ###p<0.001compared with the 1000 K group according to a one-way ANOVA with the Bonferroni post-hoc test. Sham: sham-operated.

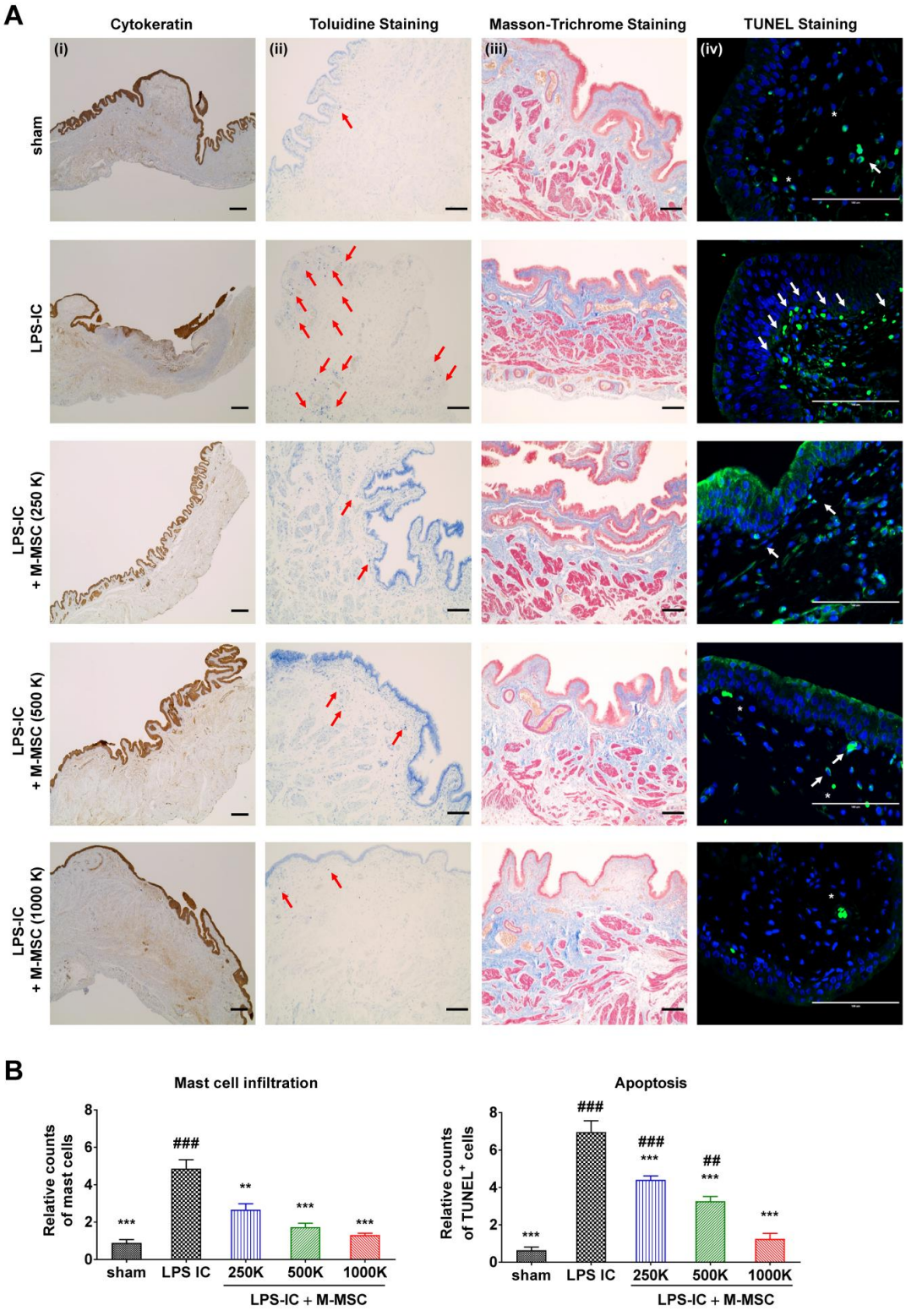
A
Cytokeratin
Toluidine Staining
Masson-Trichrome Staining
TUNEL Staining
(i)
(ii)
(iii)
(iv)
sham
LPS-IC
LPS-IC + M-MSC (250 K)
LPS-IC + M-MSC (500 K)
LPS-IC + M-MSC (1000 K)
B
Mast cell infiltration
Relative counts of mast cells
sham
LPS IC
250K
500K
1000K
LPS-IC + M-MSC
Apoptosis
Relative counts of TUNEL+ cells

Figure 14. Injection of M-MSCs ameliorates histological abnormalities in the blad ders of LPS-IC rats.

(A) (i) Cytokeratin immunostaining (magnification ×40, scale bar = 200 μm), (ii) Toluidine blue staining (magnification ×100, scale bar = 200 μm), (iii) Masson's trichrome staining (magnification ×100, scale bar = 200 μm), and (iv) TUNEL (magnification ×400, scale bar = 100 μm) of bladder tissues of LPS-IC rats at 1 week after injection of the indicated number of M-MSCs (K = a thousand) or PBS. Arrows indicate infiltrated mast cells (ii) or apoptotic cells (iv). Sham: sham-operated. **(B)** Quantification of histological staining. Three representative areas per slide were randomly selected from five independent animals. Data (n = 15) were normalized against those in sham-operated rats and are presented as the mean ± SEM. **p<0.01 and ***p<0.001 compared with the LPS-IC group; #p<0.05, ##p<0.001, and ###p<0.001 compared with the 1000 K group according to a one-way ANOVA with the Bonferroni post-hoc test.

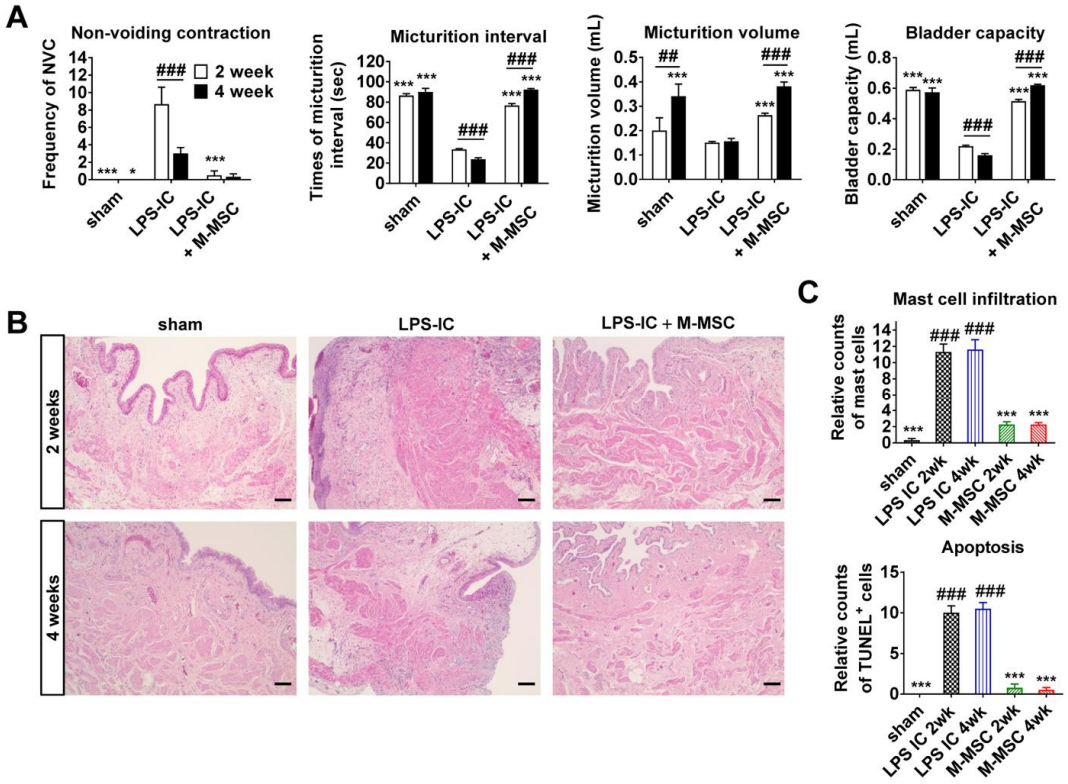

Figure 15. Long-term therapeutic effects of M-MSCs in LPS-IC rats.

(A) Quantitative bladder voiding data in LPS-IC rats at 2 and 4 weeks after injection of 1×10^6 M-MSCs. Data are presented as the mean ± SEM (six independent animals per group). **p<0.01 and ***p<0.001 compared with the LPS-IC group; ###p<0.001 for 2 weeks vs. 4 weeks according to a two-way ANOVA with the Bonferroni post-hoc test. NAC; non-voiding contraction. **(B)** Hematoxylin and eosin staining of the indicated bladder tissues (magnification ×200, scale bar = 200 μm). Nuclei were stained with Mayer's hematoxylin. **(C)** Quantification of mast cell infiltration and apoptosis in bladder tissues of LPS-IC rats at 2 and 4 weeks after injection of 1×10^6 M-MSCs. Three representative areas per slide were randomly selected from five independent animals. Data (n = 15) were normalized against

levels in sham-operated rats and are presented as the mean ± SEM. ***$p<0.001$ compared with the LPS-IC group; ###$p<0.001$ compared with the LPS-IC + M-MSC group according to a one-way ANOVA with the Bonferroni post-hoc test.

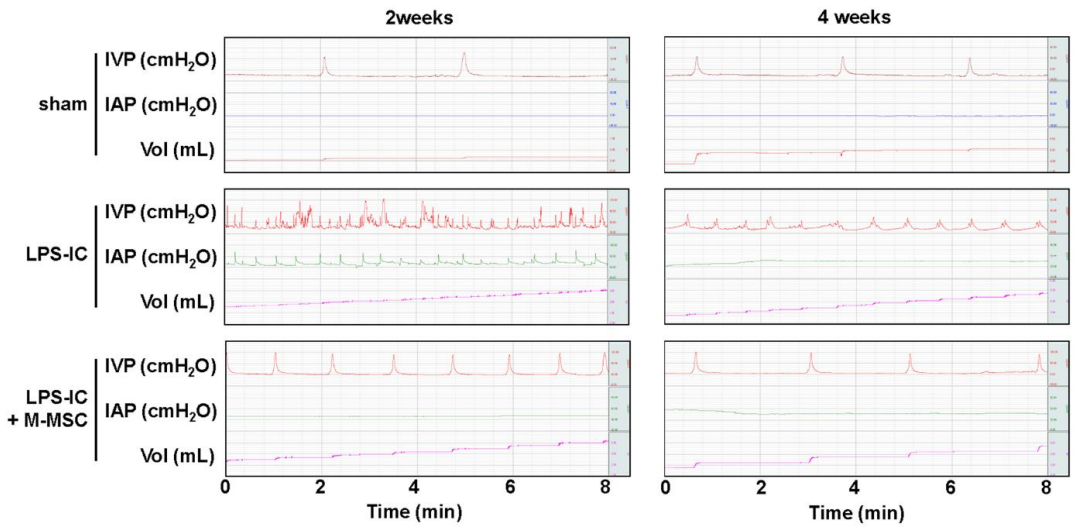

Figure 16. Long-term therapeutic effects of M-MSCs on bladder function in LPS -IC rats.

Representative awake cystometry results at 2 weeks (left) and 4 weeks (right) after injection of 1×10^6 M-MSCs (LPS-IC + M-MSC) or PBS (LPS-IC) into LPS-IC rats. Sham: sham-operated.

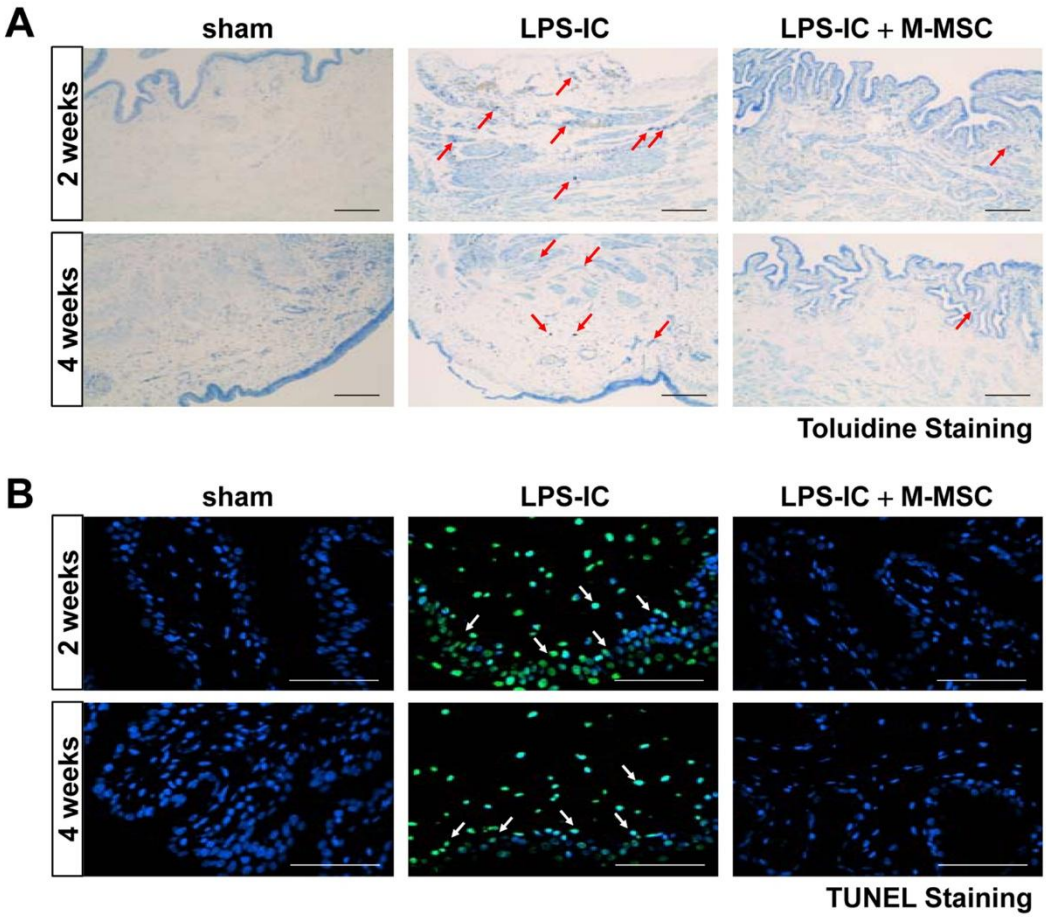

Figure 17. Therapeutic effects of M-MSCs on chronic bladder injury in LPS-IC rats.

(A and B) Representative Toluidine blue staining (**A**; magnification ×100, scale bar = 100 μm), and TUNEL (**B**; magnification ×400, scale bar = 100 μm) in bladder tissues of LPS-IC rats at 2 and 4 weeks after injection of 1×10^6 M-MSCs (LPS-IC + M-MSC) or PBS (LPS-IC). Nuclei were stained with Mayer's hematoxylin **(A)** or DAPI (blue, **B**). Arrows indicate infiltrated mast cells **(A)** and apoptotic cells **(B)**. Sham: sham-operated.

Critical role of WNT signaling on the mechanism of action for M-MSC therapy

In the HCl-induced acute IC/BPS model demonstrated previously, MSC therapy stimulated epithelial regeneration by activating sonic hedgehog (Shh) and Wnt pathways [11, 17]. In the chronic IC/BPS model, gene expression analysis revealed that the bladder tissues of LPS-IC animals characteristically down-regulate *Smoothened* (*Smo*), a transducer of Shh signaling and WNT family genes (e.g., *Wnt2b*, *Wnt4*, *Wnt5a, Wnt8a*, *Wnt8b*, and *Wnt10a*), as well as their downstream growth-factors (e.g., *Igf2*, *Fgf9*, and *Notch1*) (**Figure 18A**). This impaired gene expression was significantly ameliorated by M-MSC therapy. The activation of WNT pathways in the LPS-IC + M-MSC group was validated by the increased expression and nuclear localization of β-catenin protein, a surrogate marker for WNT signaling activation (**Figure 18B** and **Figure 19A, 19B**). In particular, the majority of the nuclear β-catenin expressing cells were in close contact with the GFP^+ engrafted cells (**Figure 18B**), suggesting that the engrafted M-MSCs enforced a microenvironment that is favorable to stimulate WNT signaling.

To validate the significance of WNT and downstream growth factor pathways, we injected indomethacin [32] or Gefitinib [33] daily. Indomethacin and Gefitinib are inhibitors for Wnt and IGF-mediated signaling activity, respectively. Both inhibitors significantly abrogated the therapeutic effects of M-MSCs to recover bladder voiding functions in LPS-IC animals (**Figure 18C**). Both molecules significantly impaired the engraftment of administrated M-MSCs (**Figure 18D** and **Figure 19C**). Thus, these results indicate that the

Wnt and IGF signaling cascades play a crucial role in the beneficial outcomes of M-MSC in treating the chronic inflammatory bladder injuries of IC/BPS bladder.

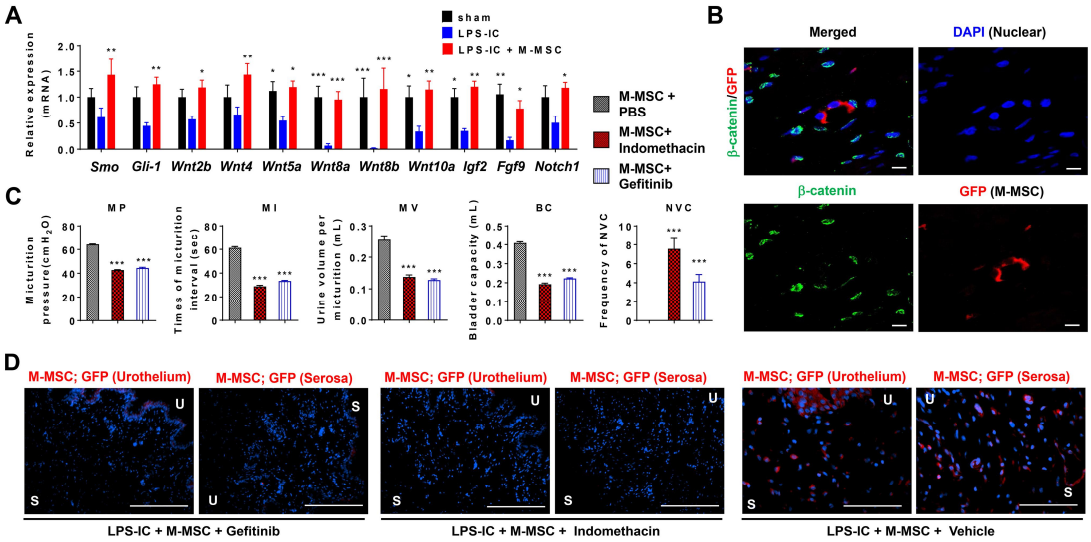

Figure 18. Role of WNT signaling in the therapeutic effects of M-MSCs.

(A) RQ-PCR analyses of the expression levels of *Shh*, *WNT*, and downstream growth factors in the bladder tissues of LPS-IC rats at 1 week after injection of 1×10^6 M-MSCs or PBS. RQ-PCR assays were performed in duplicates for five independent animals. Expression levels (n = 10) were normalized against those in sham-operated rats and are presented as the mean ± SEM. *p<0.05, **p<0.01, and ***p<0.001 compared with the LPS-IC group according to a two-way ANOVA. **(B)** Representative confocal micrographs (magnification ×1,000, scale bar = 10 μm) of bladder sections of LPS-IC rats transplanted with GFP^+ M-MSCs. Samples were co-stained for GFP (red) and β-catenin (green). Nuclei were stained with DAPI (blue). **(C)** Quantitative bladder voiding data in LPS-IC rats (eight independent animals per group) at 1 week after injection of 1×10^6 M-MSCs in the absence or presence of indomethacin or Gefitinib, which inhibit WNT and IGF-mediated signaling, respectively. All

data are presented as the mean ± SEM. ***p<0.001 compared with the LPS-IC group according to a one-way ANOVA with the Bonferroni post-hoc test. **(D)** Immunostaining of M-MSCs stably expressing GFP (red) in the bladders of the indicated rats (magnification ×200, scale bar = 200 μm). U: urothelium; S: serosa; sham: sham-operated.

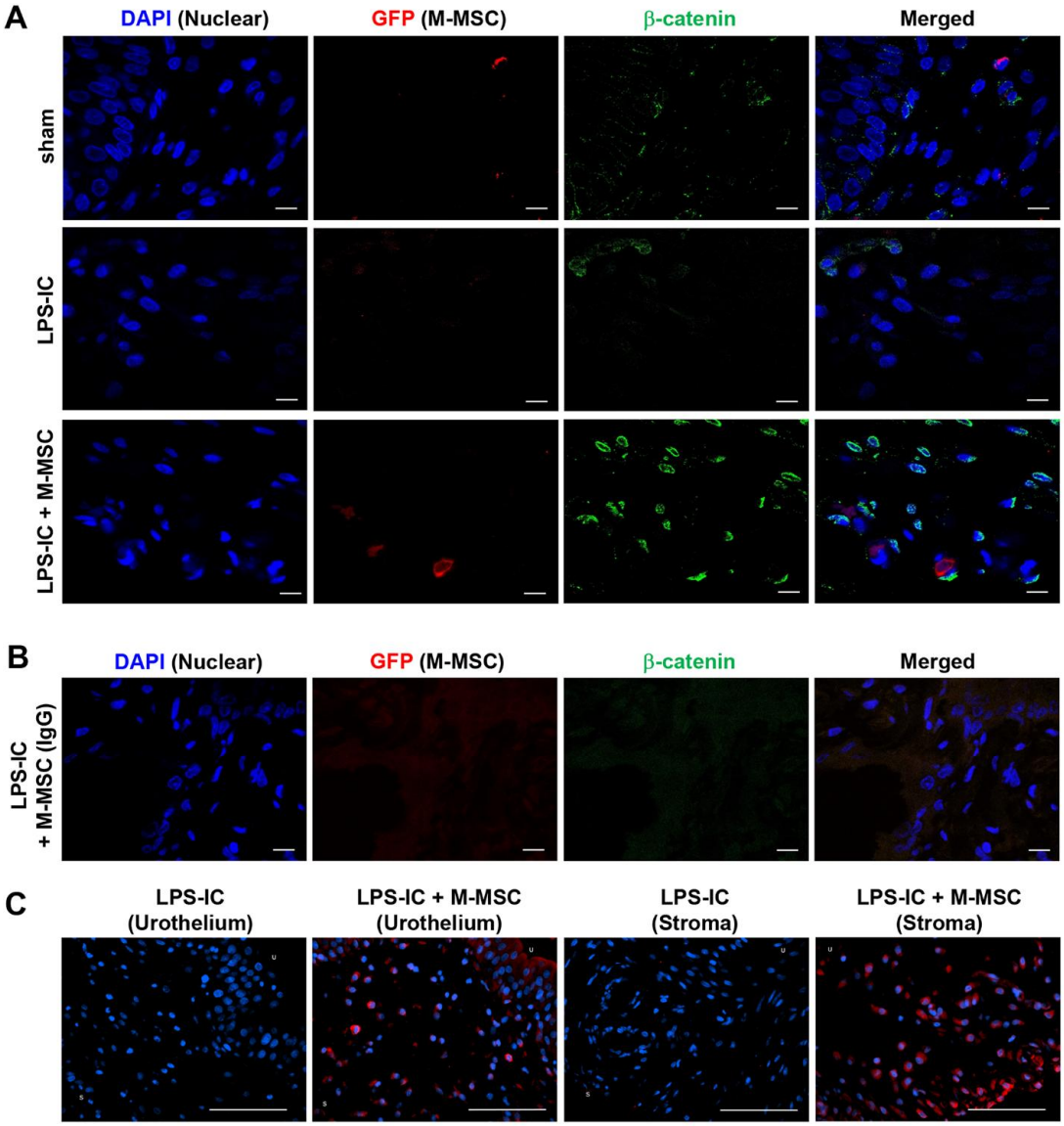

Figure 19. Immunofluorescence analysis of WNT signaling and engraftment of M-MSCs.

(A) Representative confocal micrographs of bladder sections from the indicated groups of rats co-stained for GFP (red) and β-catenin (green) (magnification ×1,000, scale bar = 10 μm). Nuclei were stained with DAPI (blue). **(B)** Bladder sections of LPS-IC + M-MSC rats were stained with mouse and rabbit IgG control antibodies as a negative control in

experiments assessing the nuclear localization of β-catenin and engraftment of GFP^+ cells (magnification ×1,000, scale bar = 10 μm). **(C)** Bladder tissues of LPS-IC rats not injected with GFP^+ M-MSCs (LPS-IC; w/o M-MSC) were stained as a negative control in experiments assessing the engraftment of GFP^+ cells (magnification ×200, scale bar = 200 μm). Nuclei were stained with DAPI (blue). U: urothelium; S: serosa; sham: sham-operated.

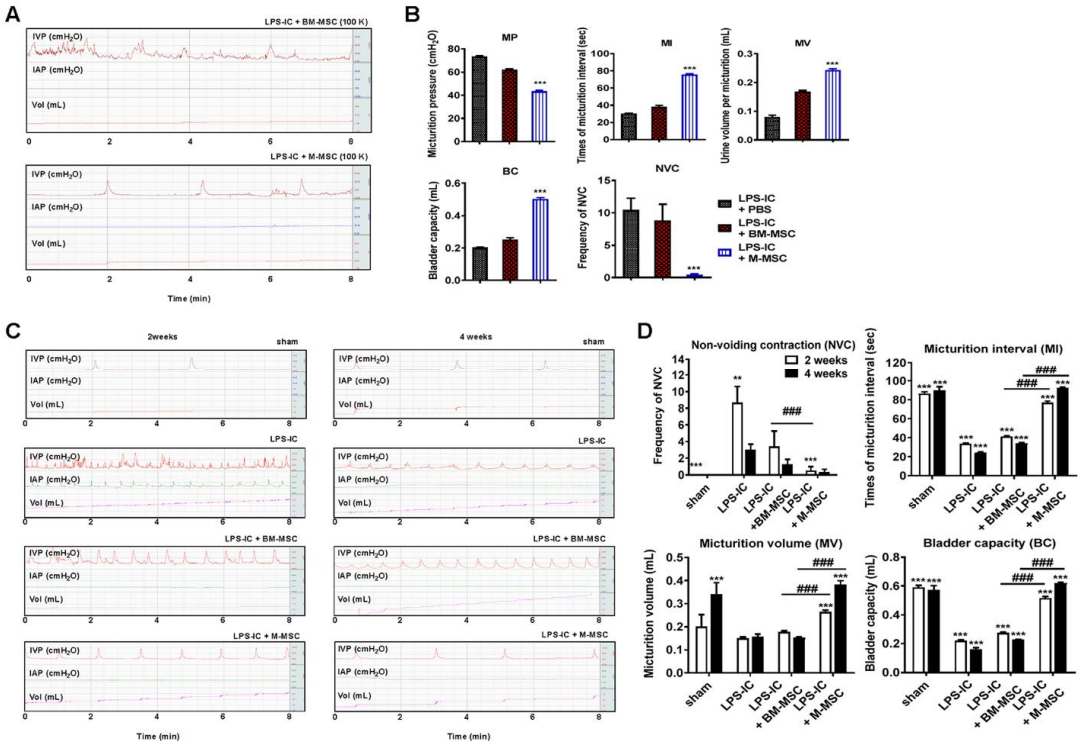

Figure 20. The therapeutic efficacy of M-MSCs is superior to that of BM-MSCs.

(A and C) Representative awake cystometry at 1 week **(A)** or 2 or 4 weeks **(C)** after injection of M-MSCs or BM-MSCs (1×10^5 cells; 100 K) into the bladders of LPS-IC rats. **(B and D)** The non-voiding contraction (NVC), micturition interval (MI), micturition volume (MV), and bladder capacity (BC) were quantified from the voiding pattern analysis. All data are presented as the mean ± SEM (five independent animals per group). Data were statistically analyzed using a one-way **(B)** or two-way **(D)** ANOVA and the Bonferroni post-hoc test. ***p<0.001 compared with the LPS-IC group; ###p<0.001 for the M-MSC vs. BM-MSC groups.

DISCUSSION

IC/BPS is regarded a heterogeneous, multifactorial disease [34, 35]. Its etiology is not fully understood and curable treatments have not been identified. Recent studies reported that IC/BPS may be present in >2% of females far more than previously considered prevalence of 0.1% [36]. Although several treatment tools have been used, many patients have persistent symptoms after the treatments by suffering poor quality of life with sleep dysfunction, sexual dysfunction, depression, anxiety and stress [37]. Therefore, treatment of IC/BPS [38, 39] remains a clinical challenge and further researches on the pathogenesis of the disease and developing the reliable animal models are significant to identify curative treatments. Recently several pathophysiologies of IC/BPS were introduced such as inflammation and mast cell activation, nitric oxide or autoimmune mechanism and glycogaminoglycan layer defect [40-43]. These multifactorial causes of IC/BPS could be effectively interfered by stem cell therapy by regenerating the denudated urothelium by direct differentiation and at the same time modulating the chronic inflammation and immune response by secreting the tropic factors.

MSC therapy has been considered a promising approach for treating IC/BPS [44]. However, a poor understanding of the mechanism of action and the *in vivo* behavior of transplanted cells has resulted in skepticism over current MSC-based therapy. We introduce MSC-based therapies to a rat model of chronic IC/BPS which builds on previous models for

longer term therapeutic results and a more accurate determination of the mechanisms of therapeutic effect. We previously reported beneficial effects of UCB-MSC for treating IC/BPS or ketamine induced cystitis [11, 12].

However, their survival in tissue was limited to a short period of one week after transplantation and the transplanted cells showed limited capacity to integrate into bladder tissues. However, the present hESCs-derived M-MSCs survived more than 1 month after transplantation. Enhanced *in vivo* engraftment and survival of M-MSCs than adult-tissue counterparts explained the superior and long-lasting therapeutic potency of these hESC progeny in treating IC/BPS.

Through a combination of immunostaining and intravital imaging we were able to verify that M-MSC beneficial results are due to WNT and IGF signalling cascades, and thus it may be speculated that the engrafted M-MSCs replenish the urothelial layer of the bladder against further self-inflicted environmental damage while contributing to a micro-environment favorable to tissue repair. The high resolution of intravital confocal imaging and microcystoscopic imaging techniques provided allowed further direct observation of differentiation of M-MSCs into perivascular cells and formation of stable multicellular structures, potentially initiating a long-term treatment effect. This positive treatment result demonstrated marked improvement in a chronic model of IC/PBS through stem cell-based treatment without any adverse safety issues. Indeed, M-MSCs showed the superior therapeutic potency to BM-MSCs in the LPS-IC animal model (**Figure 20**).

Due to the size of objective lenses, imaging with objective lenses of *in vivo* targets has previously been largely restricted to superficial tissues such as skin or surgically exposed internal organs. To overcome this drawback, we also employed an endo-microscope technique with a small-diameter graded-index (GRIN) lens probe to perform cystoscopy, accessing internal bladder tissue in a minimally invasive manner. While endoscopy only tracked well-focused engrafted cells for a limited period of time, it allowed confirmation of cellular migration to and engraftment in the urothelium, as well as limited visualization into the lamina propria. The defocusing and dimming of observed cells after 21 DAT are likely due to limitations in the focal depth of the GRIN probe and to the limited optical penetration depth of visible light-based endoscopy to ~100 μm in most soft tissues, respectively.

Due to limitations of the observation area of the GRIN probe and confocal objective, it was not possible to verify dispersal of injected stem cells over the entire bladder. However, the chronic model of IC/BPS was not targeted to specific bladder regions and impacts the entire urothelium equally; cystometry revealed improvement in bladder regulation, and outcomes which was not limited to the single point of MSC injection. We observed migration of M-MSCs from the bladder serosa, where the MSCs were injected, to the highly damaged urothelium over a three-day period, which is the first confirmed observation of stem cell migration benefitting therapeutic treatment in living bladder models of IC/BPS, to the best knowledge of the authors. We speculate that between the 3 and 7 DAT the observed decrease in fluorescence intensity and M-MSC cell count may be due to dispersal of M-MSCs over

the whole bladder.

After tracing the migration of transplanted M-MSC from the bladder serosa to the mucosa over a seven-day period, *in vivo* cellular differentiation in the urothelium, lamina propria, and serosa was observed, as well as subsequent differentiation of M-MSC cells into endothelial, and epithelial over a 30 day period, which correlated with improvement in IC/BPS symptoms including bladder denudation and NVC in the animal of the LPS-IC + M-MSC group.

Of importance, the transplanted M-MSCs clearly integrated into functional compartments of the bladder including E-cadherin^{+} urothelial cells, CD31^{+} endothelial cells and vimentin^{+} stromal or pericytes. In particular, the engrafted cells in the lamina propria and partly to the urothelium stimulate WNT-related epithelial regeneration capacity. Thus, the functional integration of transplanted M-MSCs might effectively remedy the chronic inflammatory IC/BPS injury by restoring the urothelial barrier function to protect the bladder from leaking of urine and at the same time by boosting the immune-modulatory and anti-inflammatory microenvironments. Furthermore, well-controlled *in vitro* differentiation could strengthen *in vivo* survival, engraftment, and functionality of hESC-derivatives [19].

In our previous study using HCl-induced IC/BPS animal model, the engrafted M-MSCs was observed until 6 months after transplantation [17]. Unlike the previous acute model, the engrafted M-MSCs in the LPS-IC animals were hardly observed 6 weeks after transplantation in intravital imaging (**Figure 4, Figure 6**) or in the immuno-histological

analysis (**Figure 12**). The different tissue microenvironments between acute (HCl instillation) and chronic (LPS instillation) IC injuries could determine the potency of engraftment and integration of the transplanted M-MSCs. Although no adverse outcomes relating to immune rejection and tissue inflammation were observed during our experimental period, the distinct immune responses between two animal models could contribute to the different *in vivo* biological dynamics of the xenogenic transplanted cells. Previously, we proved that hESCs and their differentiated derivatives showed little immunogenic potency because of little expression of immunologically relevant cell surface markers, including HLA-DR and costimulatory molecules (CD40, CD40L, B7-1, and B7-2) [17, 20, 45]. Despite little immunogenicity of M-MSCs, the impact of the immune response to the engrafted M-MSCs in the pathological bladders should be carefully investigated in a further study.

CONCLUSION

In the present study, using a combination of longitudinal intravital confocal imaging and microcystoscopy, we characterized the distributions, properties, and intercellular interactions of the hESC-derived M-MSCs *in vivo* after transplantation of them in an animal model of chronic IC/BPS. We monitored the migration and differentiation of transplanted M-MSCs in the urothelium and demonstrated that the WNT and IGF signaling cascades are involved in the long-term therapeutic effects of these cells. Since the biological properties of engrafted stem cells, including transcriptional activity, external signal transduction, and differentiation potency, may vary according to the environment [46], the present study about longitudinal analysis of engrafted cells in living animals may help to advance our understanding of the cellular mechanisms underlying functional improvement, clarify the risk of tumorigenesis after transplantation, and optimize transplantation protocols prior to clinical trials.

REFERENCE

1. Bianco, P., Cao, X., Frenette, P.S., Mao, J.J., Robey, P.G., Simmons, P.J., and Wang, C.Y. (2013). The meaning, the sense and the significance: translating the science of mesenchymal stem cells into medicine. Nature medicine *19*, 35-42.
2. Jaing, T.-H. (2014). Umbilical Cord Blood: A Trustworthy Source of Multipotent Stem Cells for Regenerative Medicine. Cell Transplantation *23*, 493-496.
3. Damien, P., and Allan, D.S. (2015). Regenerative Therapy and Immune Modulation Using Umbilical Cord Blood–Derived Cells. Biology of Blood and Marrow Transplantation *21*, 1545-1554.
4. Knaän-Shanzer, S. (2014). Concise Review: The Immune Status of Mesenchymal Stem Cells and Its Relevance for Therapeutic Application. STEM CELLS *32*, 603-608.
5. Bianco, P., Cao, X., Frenette, P.S., Mao, J.J., Robey, P.G., Simmons, P.J., and Wang, C.-Y. (2013). The meaning, the sense and the significance: translating the science of mesenchymal stem cells into medicine. Nature medicine *19*, 35-42.
6. Hyunsuk, J., lt, sup, gt, lt, sup, gt, Hyeon Woo, Y., lt, sup, et al. (0000). Mesenchymal Stem Cell Therapy for Ischemic Heart Disease: Systematic Review and Meta-analysis. International Journal of Stem Cells *0*.
7. Wezel, F., Southgate, J., and Thomas, D.F.M. (2011). Regenerative medicine in urology. BJU International *108*, 1046-1065.
8. Kim, A., Shin, D.-M., and Choo, M.-S. (2015). Stem Cell Therapy for Interstitial Cystitis/Bladder Pain Syndrome. Current Urology Reports *17*, 1-9.
9. Propert, K.J., Schaeffer, A.J., Brensinger, C.M., Kusek, J.W., Nyberg, L.M., and Landis, J.R. (2000). A prospective study of interstitial cystitis: results of longitudinal followup of the interstitial cystitis data base cohort. The Interstitial Cystitis Data Base Study Group. J Urol *163*, 1434-1439.

10. Oravisto, K.J. (1975). Epidemiology of interstitial cystitis. Ann Chir Gynaecol Fenn *64*, 75-77.

11. Song, M., Lim, J., Yu, H.Y., Park, J., Chun, J.-Y., Jeong, J., Heo, J., Kang, H., Kim, Y., Cho, Y.M., et al. (2015). Mesenchymal Stem Cell Therapy Alleviates Interstitial Cystitis by Activating Wnt Signaling Pathway. Stem Cells and Development *24*, 1648-1657.

12. Kim, A., Yu, H.Y., Heo, J., Song, M., Shin, J.-H., Lim, J., Yoon, S.-J., Kim, Y., Lee, S., Kim, S.W., et al. (2016). Mesenchymal stem cells protect against the tissue fibrosis of ketamine-induced cystitis in rat bladder. Scientific Reports *6*, 30881.

13. Cheng, A.S., and Yau, T.M. (2008). Paracrine Effects of Cell Transplantation: Strategies to Augment the Efficacy of Cell Therapies. Seminars in Thoracic and Cardiovascular Surgery *20*, 94-101.

14. Maltais, S., Tremblay, J., Perrault, L., and Ly, H. (2010). The Paracrine Effect: Pivotal Mechanism in Cell-Based Cardiac Repair. J. of Cardiovasc. Trans. Res. *3*, 652-662.

15. Gharaibeh, B., Lavasani, M., Cummins, J., and Huard, J. (2011). Terminal differentiation is not a major determinant for the success of stem cell therapy - cross-talk between muscle-derived stem cells and host cells. Stem Cell Research & Therapy *2*, 31.

16. Kim, J.K., Lee, W.M., Kim, P., Choi, M., Jung, K., Kim, S., and Yun, S.H. (2012). Fabrication and operation of GRIN probes for in vivo fluorescence cellular imaging of internal organs in small animals. Nat. Protocols *7*, 1456-1469.

17. Kim, A., Yu, H.Y., Lim, J., Ryu, C.-M., Kim, Y.H., Heo, J., Han, J.-Y., Lee, S., Bae, Y.S., Kim, J.Y., et al. (2017). Improved efficacy and in vivo cellular properties of human embryonic stem cell derivative in a preclinical model of bladder pain syndrome. Scientific Reports *7*, 8872.

18. Song, M., Heo, J., Chun, J.-Y., Bae, H.S., Kang, J.W., Kang, H., Cho, Y.M., Kim, S.W., Shin, D.-M., and Choo, M.-S. (2013). The Paracrine Effects of Mesenchymal Stem Cells Stimulate the Regeneration Capacity of Endogenous St

em Cells in the Repair of a Bladder-Outlet-Obstruction-Induced Overactive Bla dder. Stem Cells and Development *23*, 654-663.

19. Kim, J.M., Hong, K.S., Song, W.K., Bae, D., Hwang, I.K., Kim, J.S., and Ch ung, H.M. (2016). Perivascular Progenitor Cells Derived From Human Embryo nic Stem Cells Exhibit Functional Characteristics of Pericytes and Improve the Retinal Vasculature in a Rodent Model of Diabetic Retinopathy. Stem Cells Transl Med *5*, 1268-1276.
20. Hong, K.-S., Bae, D., Choi, Y., Kang, S.-W., Moon, S.-H., Lee, H.T., and Ch ung, H.-M. (2014). A Porous Membrane-Mediated Isolation of Mesenchymal S tem Cells from Human Embryonic Stem Cells. Tissue Engineering Part C: Me thods *21*, 322-329.
21. Kim, Y., Jin, H.J., Heo, J., Ju, H., Lee, H.Y., Kim, S., Lee, S., Lim, J., Jeon g, S.Y., Kwon, J., et al. (2018). Small hypoxia-primed mesenchymal stem cell s attenuate graft-versus-host disease. Leukemia.
22. Lee, T., and Yoon, S.M. (2013). The Role of Intra-abdominal Pressure Measur ement in Awake Rat Cystometry. Int Neurourol J *17*, 44-47.
23. Jin, L.H., Shin, H.Y., Kwon, Y.H., Park, C.S., Yoon, S.M., and Lee, T. (201 0). Urodynamic findings in an awake chemical cystitis rat model observed by simultaneous registrations of intravesical and intraabdominal pressures. Int Ne urourol J *14*, 54-60.
24. Jin, J.H., Lee, H.J., Heo, J., Lim, J., Kim, M., Kim, M.K., Nam, H.Y., Hong, G.H., Cho, Y.S., Choi, S.J., et al. (2015). Senescence associated MCP-1 secr etion is dependent on a decline in BMI1 in human mesenchymal stromal cell s. Antioxid. Redox Signal.
25. Jeong, E.M., Yoon, J.H., Lim, J., Shin, J.W., Cho, A.Y., Heo, J., Lee, K.B., Lee, J.H., Lee, W.J., Kim, H.J., et al. (2018). Real-Time Monitoring of Glutat hione in Living Cells Reveals that High Glutathione Levels Are Required to Maintain Stem Cell Function. Stem Cell Reports.
26. Stein, P.C., Pham, H., Ito, T., and Parsons, C.L. Bladder Injury Model Induce d in Rats by Exposure to Protamine Sulfate Followed by Bacterial Endotoxin.

The Journal of Urology *155*, 1133-1138.

27. Birder, L., and Andersson, K.-E. (2018). Animal Modelling of Interstitial Cystitis/Bladder Pain Syndrome. Int Neurourol J *22*, S3-9.

28. Lilly, J.D., and Parsons, C.L. (1990). Bladder surface glycosaminoglycans is a human epithelial permeability barrier. Surgery, gynecology & obstetrics *171*, 493-496.

29. Shie, J.H., and Kuo, H.C. (2011). Higher levels of cell apoptosis and abnormal E-cadherin expression in the urothelium are associated with inflammation in patients with interstitial cystitis/painful bladder syndrome. BJU Int *108*, E136-141.

30. Logadottir, Y., Delbro, D., Fall, M., Gjertsson, I., Jirholt, P., Lindholm, C., and Peeker, R. (2014). Cytokine expression in patients with bladder pain syndrome/interstitial cystitis ESSIC type 3C. J Urol *192*, 1564-1568.

31. Sant, G.R., Kempuraj, D., Marchand, J.E., and Theoharides, T.C. (2007). The mast cell in interstitial cystitis: role in pathophysiology and pathogenesis. Urology *69*, 34-40.

32. Dihlmann, S., Siermann, A., and von Knebel Doeberitz, M. (2001). The nonsteroidal anti-inflammatory drugs aspirin and indomethacin attenuate beta-catenin/TCF-4 signaling. Oncogene *20*, 645-653.

33. van der Poel, H.G. Smart Drugs in Prostate Cancer. European Urology *45*, 1-17.

34. Chancellor, M.B., and Yoshimura, N. (2004). Treatment of interstitial cystitis. Urology *63*, 85-92.

35. Baker, S.C., Shabir, S., Georgopoulos, N.T., and Southgate, J. (2016). Ketamine-Induced Apoptosis in Normal Human Urothelial Cells: A Direct, N-Methyl-d-Aspartate Receptor-Independent Pathway Characterized by Mitochondrial Stress. The American journal of pathology *186*, 1267-1277.

36. Clemens, J.Q., Link, C.L., Eggers, P.W., Kusek, J.W., Nyberg, L.M., Jr., McKinlay, J.B., and Investigators, B.S. (2007). Prevalence of painful bladder symptoms and effect on quality of life in black, Hispanic and white men and wom

en. J Urol *177*, 1390-1394.

37. Nickel, J.C., Tripp, D.A., Pontari, M., Moldwin, R., Mayer, R., Carr, L.K., D oggweiler, R., Yang, C.C., Mishra, N., and Nordling, J. (2010). Psychosocial phenotyping in women with interstitial cystitis/painful bladder syndrome: a cas e control study. J Urol *183*, 167-172.

38. Jhang, J.F., Birder, L.A., Chancellor, M.B., and Kuo, H.C. (2016). Patient cha racteristics for different therapeutic strategies in the management ketamine cyst itis. Neurourology and urodynamics.

39. Ha, T., and Xu, J.H. (2017). Interstitial cystitis intravesical therapy. Translatio nal Andrology and Urology, S171-S179.

40. Mullins, C., Bavendam, T., Kirkali, Z., and Kusek, J.W. (2015). Novel researc h approaches for interstitial cystitis/bladder pain syndrome: thinking beyond th e bladder. Transl Androl Urol *4*, 524-533.

41. Belknap, S., Blalock, E., and Erickson, D. (2015). The Challenges of Interstiti al Cystitis: Current Status and Future Prospects. Drugs *75*, 2057-2063.

42. Maeda, D., Akiyama, Y., Morikawa, T., Kunita, A., Ota, Y., Katoh, H., Niimi, A., Nomiya, A., Ishikawa, S., Goto, A., et al. (2015). Hunner-Type (Classic) Interstitial Cystitis: A Distinct Inflammatory Disorder Characterized by Pancy stitis, with Frequent Expansion of Clonal B-Cells and Epithelial Denudation. P LoS One *10*, e0143316.

43. Kim, A., Hoe, K.-O., Shin, J.H., and Choo, M.-S. (2017). Evaluation of the i ncidence and risk factors associated with persistent frequency in interstitial cy stitis/bladder pain syndrome and the efficacy of antimuscarinic treatment. Inve stig Clin Urol *58*, 353-358.

44. Kim, A., Shin, D.M., and Choo, M.S. (2016). Stem Cell Therapy for Interstiti al Cystitis/Bladder Pain Syndrome. Curr Urol Rep *17*, 1.

45. Lee, S.W., Ryu, C.-M., Shin, J.-H., Choi, D., Kim, A., Yu, H.Y., Han, J.-Y., Lee, H.-Y., Lim, J., Kim, Y.H., et al. (2018). The Therapeutic Effect of Hum an Embryonic Stem Cell-Derived Multipotent Mesenchymal Stem Cells on Ch emical-Induced Cystitis in Rats. Int Neurourol J *22*, S34-45.

46. Kumamaru, H., Ohkawa, Y., Saiwai, H., Yamada, H., Kubota, K., Kobayakawa, K., Akashi, K., Okano, H., Iwamoto, Y., and Okada, S. (2012). Direct isolation and RNA-seq reveal environment-dependent properties of engrafted neural stem/progenitor cells. Nat Commun *3*, 1140.

국문초록

간질성 방광염 / 방광 통증 증후군을 타겟으로 하는 줄기세포 치료를 위한
생체 내 분포 및 이식 된 세포의 특성 모니터링

간질성방광염 (interstitial cystisis, IC)은 구상화와 Hunner 궤양 같은 특징적인 방광경소견과 염증 유도 비만세포 (mast cell)군집의 조직학적 소견이 있는 방광통증증후군 질환이며, 심각한 방광염증반응과 요로상피기능장애가 특징이다.

아직까지 질환의 메커니즘이 명확하지 않으므로, 확실한 치료법이 없는 난치성 질환이며 간질성방광염 환자들은 심각한 치부 통증과 빈뇨 (20-50 번/일) 증상 때문에 정상적인 일상생활을 할 수 없는 심각한 질환이다.

확실한 치료법 부재로 간질성방광염 환자들이 일생 동안 겪게 되는 극심한 고통을 해결하기 위하여 “줄기세포치료법 기반 신규 치료법 개발” 연구가 절실한 실정이다.

본 연구진은 이전 논문에서 HCl 주입 유도 간질성방광염 질환 모델에서 MSC 줄기세포 치료 연구 및 기전을 규명하였다. 하지만 단기간에 강한 화학적 화상으로 인한 acute model 이라는 한계점을 가지고 있어 본 연구에서는 protamine sulfate (PS)와 lipopolysacchariede (LPS)를 투여하는 새로운 모델을 확립하였다. PS 는 IC 환자의 중요 병인으로 받아들여지고 있는 방광 내벽의 glycosaminoglycan (GAG) layer 손상을 유도하기 위해 사용하였고, LPS 는 박테리아의 내벽 인자로서 IC 의 또 다른 중요 병인인 inflammation 을 유발시키는

목적으로 사용하였다. 이 두 인자를 함께 사용함으로서 실제 IC disease 에 가장 적합한 모델을 형성했다고 판단된다. 8 주령의 SD rat 을 이용하여 5 주동안 LPS 와 PS 를 방광 내에 주입하여 IC 를 유발시키고, M-MSC 줄기세포를 방광 내벽에 단회 투여하고 일주일 뒤, 방광기능평가, 조직학적 검사 및 방광 조직의 유전자 발현 측정을 실시하였다. Awake cystomery 을 통한 방광기능검사와 H&E 염색을 통한 조직학적 검사 결과, M-MSC 단회 투여로 LPS-IC 질환모델에서 간질성방광염의 방광 기능 이상과 병리학적 소견들이 모두 호전되는 것을 확인하여 LPS-IC 간질성방광염에 대한 M-MSC 줄기세포 전임상 효능을 확인하였다. 또한 생체 내 공초점 내시경 및 현미경 (Intravital confocal endoscope or microscopy) 이미징 기법을 활용하여, GFP 형광단백질로 표식된 인간 배아줄기세포 유래 다분화성 MSC 을 백서 모델에 이식한 후, 이식 후 생착 세포 생체 내 특성 분석을 42 일 동안 장기 모니터링 함으로써 줄기세포 이식 후 생체 동태 분석 및 유효적 치료 기전 (MoA)의 근거 자료를 확보하였다.

따라서 본 연구를 통해 방광기능이상 질환모델, 마이크로 내시경 기술을 융합한 방광질환 타겟 줄기세포 치료법의 전임상 효능 모니터링 기법을 개발하여 글로벌 수준의 줄기세포 치료법 실용화를 위한 기반을 구축하고 임상 진입 근거를 확보하여 난치성 질환 극복을 위한 차세대 줄기세포-재생의료 치료/진단 기술 마련과 이를 통한 임상연구 강화 및 실용화를 촉진할 수 있을 것이라 기대된다.